Geoscience Frontiers 15 (2024) 101802

Contents lists available at ScienceDirect

Geoscience Frontiers

journal homepage: www.elsevier.com/locate/gsf

Research Paper

Enhancing landslide susceptibility mapping incorporating landslide typology via stacking ensemble machine learning in Three Gorges Reservoir, China

Lanbing Yu [a], Yang Wang [a,b], Biswajeet Pradhan [c,d,*]

[a] Faculty of Engineering, China University of Geosciences, Wuhan 430074, China
[b] Research Center of Geohazard Monitoring and Warning in the Three Gorges Reservoir, Chongqing 404199, China
[c] Centre for Advanced Modelling and Geospatial Information Systems (CAMGIS), School of Civil and Environmental Engineering, Faculty of Engineering and IT, University of Technology Sydney, Ultimo, NSW 2007, Australia
[d] Earth Observation Centre, Institute of Climate Change, Universiti Kebangsaan Malaysia, 43600 UKM, Bangi, Selangor, Malaysia

ARTICLE INFO

Article history:
Received 6 September 2023
Revised 9 December 2023
Accepted 26 January 2024
Available online 29 January 2024
Handling Editor: Wengang Zhang

Keywords:
Landslide susceptibility mapping
Deep learning model
Landslide types
Stacking method

ABSTRACT

Different types of landslides exhibit distinct relationships with environmental conditioning factors. Therefore, in regions where multiple types of landslides coexist, it is required to separate landslide types for landslide susceptibility mapping (LSM). In this paper, a landslide-prone area located in Chongqing Province within the middle and upper reaches of the Three Gorges Reservoir area (TGRA), China, was selected as the study area. 733 landslides were classified into three types: reservoir-affected landslides, non-reservoir-affected landslides, and rockfalls. Four landslide inventory datasets and 15 landslide conditional factors were trained by three Machine Learning models (logistic regression, random forest, support vector machine), and a Deep Learning (DL) model. After comparing the models using receiver operating characteristics (ROC), the landslide susceptibility indexes of three types landslides were acquired by the best performing model. These indexes were then used as input to generate the final map based on the Stacking method. The results revealed that DL model showed the best performance in LSM without considering landslide types, achieving an area under the curve (AUC) of 0.854 for testing and 0.922 for training. Moreover, when we separated the landslide types for LSM, the AUC improved by 0.026 for testing and 0.044 for training. Thus, this paper demonstrates that considering different landslide types in LSM can significantly improve the quality of landslide susceptibility maps. These maps in turn, can be valuable tools for evaluating and mitigating landslide hazards.

1. Introduction

Landslides are recognized as a global geohazard that can cause immense damage to the natural environment, social security, and human lives (Dai et al., 2002; Samia et al., 2017). As an integral part of landscape evolution, landslides can be viewed as a continuous, ever-evolving system, encompassing the past, present, and future (Reichenbach et al., 2018; Temme et al., 2020). Therefore, researchers often analyze the relationship between historical landslides and environmental factors to predict potential landslide occurrences in the future (Guzzetti et al., 2005), which is known as landslide susceptibility.

In the recent decades, landslide susceptibility mapping (LSM) has become an essential component of hazard assessment and emergency management, leading to numerous studies focusing in this field (Huang et al., 2022; Loche et al., 2022). Over the last couple of decades, various models have been employed for LSM, which can be broadly categorized into three types: physically-based models, knowledge-driven models, and data-driven models. Physically-based models are usually used for modelling at small scales, allowing for a detailed examination of landslide stability and movement processes based on physical equations (Tofani et al., 2017; Medina et al., 2021). However, they require numerous detailed parameters, such as unit weight of soil, cohesion, shear strength angle, and others (van den Bout et al., 2022). Knowledge-driven models, on the other hand, rely on expert knowledge to generate reliable

* Corresponding author at: Centre for Advanced Modelling and Geospatial Information Systems (CAMGIS), School of Civil and Environmental Engineering, Faculty of Engineering and IT, University of Technology Sydney, Ultimo, NSW 2007, Australia.
E-mail address: Biswajeet.Pradhan@uts.edu.au (B. Pradhan).

https://doi.org/10.1016/j.gsf.2024.101802

susceptibility maps by understanding the relationship between landslides and inducing factors in a particular area (Zhu et al., 2014). These models perform well in regions with limited historical landslide inventory, employing methods such as heuristic model, and multi-criteria decision analysis, among others (Erener et al., 2016; Du et al., 2020). Data-driven models encompass three main branches: statistical models, machine learning (ML) models, and deep learning (DL) models. The effectiveness of these models largely depends on the availability of a landslide inventory and a detailed input feature database (Lee and Min, 2001). Statistical models, for instance, can calculate specific statistical indices that reflect the internal response of landslides to predisposing factors (Liao et al., 2022). Various models, such as the information value (IV) model, weights of evidence model, and logistic regression (LR) model, have been proposed and applied to ascertain landslide susceptibility in different regions worldwide (Choi et al., 2012; Sharma et al., 2015).

Recently, numerous studies have highlighted higher prediction accuracies of ML models compared to statistical models (Merghadi et al., 2020; Al-Najjar and Pradhan, 2021). ML models have gained widespread adoption LSM due to their strong ability to fit complex nonlinear relationships. Some commonly used ML models for LSM include Bayesian networks (Tien Bui et al., 2016), support vector machines (SVM) (Marjanović et al., 2011), random forest (Dou et al., 2019; Zhou et al., 2021) (RF), artificial neural network (Gorsevski et al., 2016), and boosted regression tree (Lombardo et al., 2015). With the rapid development of soft computing techniques, a variety of ensemble learning algorithms and ensemble classifiers have been proposed to conduct LSM (Zhang et al., 2022a), such as eXtreme Gradient Boosting (XGBoost) (Wang et al., 2023; Zhang et al., 2023). For specific task of LSM, the predictive accuracy of different ML models can vary significantly due to their diverse characteristics and limitations in a given area. As a result, many investigators compare two or more different ML models, and then generate the LS map using the best preforming model (Oh and Pradhan, 2011; Hong et al., 2016). More recently, DL algorithms have shown significant breakthroughs in various fields, and the most popular DL algorithms in LSM include Convolutional Neural Networks (CNN) (Youssef et al., 2022), Recurrent Neural Network (Yuan and Chen, 2022), Deep Neural Network (Aslam et al., 2023), Gated Recurrent Unit Network (Zhang et al., 2022b). Despite DL models demonstrating higher accuracy compared to conventional ML models and statistic models, the complex modelling techniques of DL models still require further exploration in LSM.

However, landslides in a given area often comprise different geotechnical materials (e.g. soil, rock, debris, ice), and can manifest in different movement types, including sliding, falling, toppling, flowing, and spreading (Epifânio et al., 2014; Hungr et al., 2014; Camera et al., 2021). Previous researches have demonstrated that different types of landslides have distinct relationships with conditioning factors (Thiery et al., 2007; Valdés Carrera et al., 2022). For instance, Zhou et al. (2018) demonstrated that colluvial landslides and rockfalls are most influenced by the distance from roads and altitude. Similarly, Bera et al. (2021) found that in a landslide-prone area in Sikkim Himalaya, India, slope plays the most significant role in rockfalls with an IV of 34.92, while soil depth has the most impact on debris flows with an IV of 28.54. This observation necessitates the consideration of different types of landslides in landslide susceptibility assessment. Despite the vast literature on LSM, relatively few studies have emphasized landslide typology in LSM. For example, Shou and Chen (2021) individually generated the susceptibility maps of deep-seated and shallow landslides in Taiwan, Zêzere (2002) assessed the susceptibility of shallow translational slides, deep translational movements, and rotation movements in the area North of Lisbon. In another work, Silva et al. (2018) quantified the susceptibility of falls and slides in Flores Island, Azores archipelago North Atlantic Ocean. Nevertheless, these studies focused solely on generating a set of susceptibility maps for different types of landslides, without achieving a better overall map by considering landslide types collectively. Hence, LSM considering landslide types remains a challenge and warrants attention, especially in regions where multiple types of landslides coexist.

During periods of reservoir water fluctuation or the rainstorm season, various types of landslides occur in the Three Gorges Reservoir area (TGRA), posing a significant threat to the residents (Tang et al., 2019; Zhou et al., 2022a, 2022b). Despite numinous previous studies on LSM in the TGRA, none have considered landslide types. To address this gap, this study proposed a new stacking framework to integrate different types of landslides, and a landslide-prone area located in the middle and upper reaches of TGRA was selected as the test area. Landslides in this region were categorized into reservoir-affected landslides, non-reservoir-affected landslides, and rockfalls. LSM was conducted for each of the three types of landslides using LR, RF, SVM, and DL model (Resnet-18), respectively. Additionally, LSM was performed for all landslides collectively. By validating the models using the AUC value, the susceptibility of three types landslides was calculated using the best individual model. Subsequently, a map considering all landslide types was produced by stacking the susceptibility maps of each type. This paper aims to improve the reliability and scientific rigor of the LSM with these results. The findings are expected to provide a reliable basis for future site layout planning and road line selection in the area.

2. Study area

The study area is located in Chongqing Province, southwestern China, in the middle and upper reaches of the TGRA (Fig. 1). Geographically, it extends between 107°55′22″E, 30°24′25″N and 108°53′25″E, 31°14′58″N, covering an area of nearly 3457 km^2, with altitude ranging from 200 to 1400 m. The climate is characterized as subtropical monsoon, with an annual average precipitation ranging from 1050 to 1700 mm, and an average yearly temperature of 10 to 18 °C. Most rainfall is concentrated in the monsoon season, typically occurring between May and September. According to data from the China Meteorological Administration (https://data.cma.cn), the maximum monthly precipitation of 711.8 mm occurred in July 1982, and the maximum daily precipitation of 243.3 mm occurred on July 16, 2007.

Geologically, the study area is situated in the typical ejective fold mountain region of the eastern Sichuan basin (Fig. 2a). It is characterized by narrow and steep anticlines with broad synclines (Fig. 2b) (Hu et al., 2009). The study area features a series of arc-shaped fold structures that are parallel to the Yangtze River, trending at 70°–80° and convex to the northwest. Jurassic red beds ($J_{2\text{-}3}$) cover 78.15% of the study area, except for the Triassic limestone exposed in the core of the Tiefeng anticline and Fangdou anticline. Due to the Yanshanian tectonic activity between 170 and 70 Ma, the block has experienced prolonged uplift, leading to varying degrees of erosion of the upper Jurassic strata, while the middle and lower strata have developed relatively fully with continuous deposition (Xu et al., 2017). The lithology mainly comprises sandstone, mudstone, shale, shell shale, and limestone. There is slight metamorphism, and no igneous intrusion.

The topography of this region is influenced by several factors, including lithology, the uplift and deformation process of folds, and the erosion by rivers, characterized by a parallel ridge-and-valley area (Xiao et al., 2019). The newer formations (mudstones and shales) in the syncline core are more susceptible to erosion, forming broad platform-like hills. In contrast, the older and more

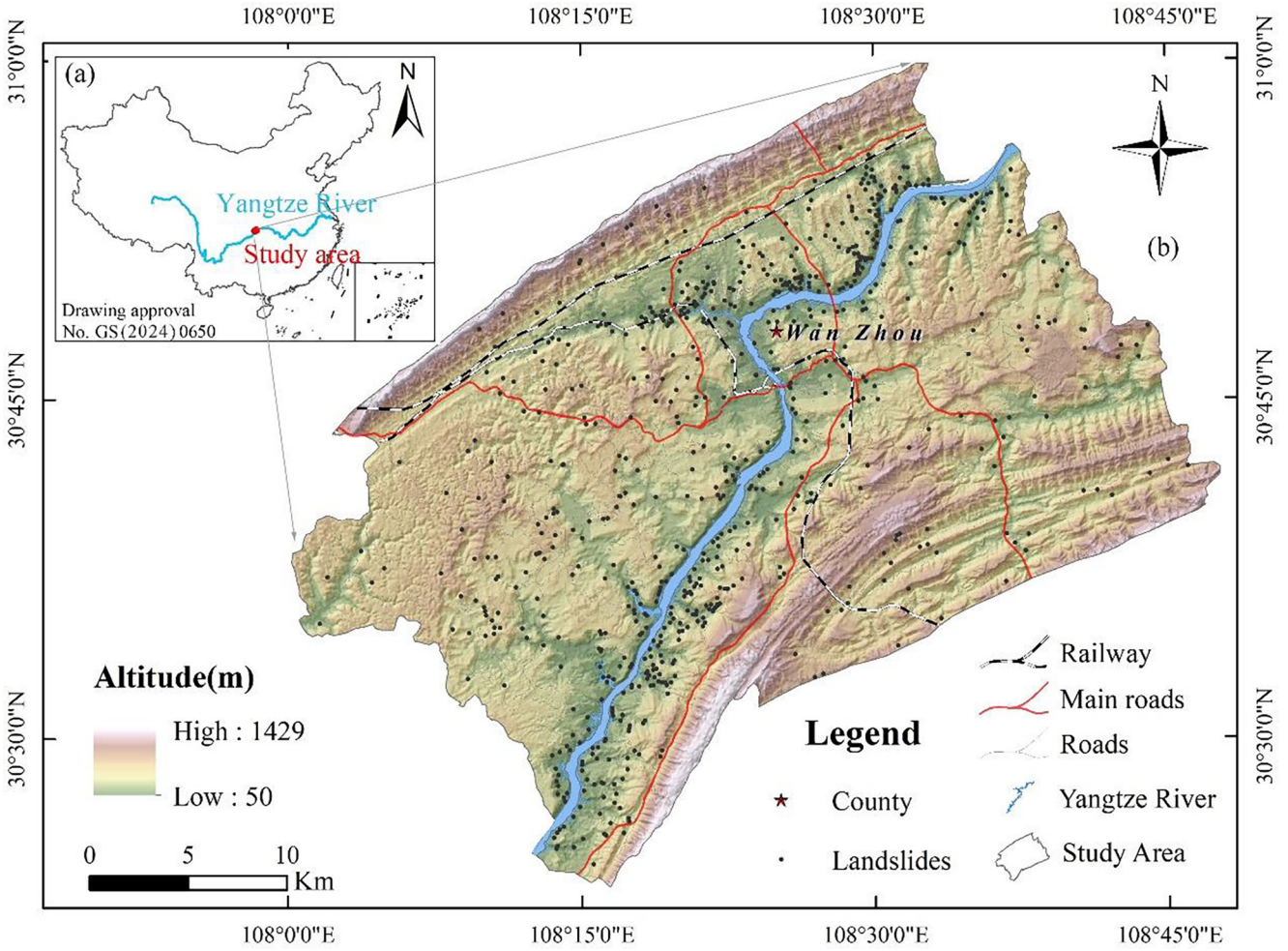

Fig. 1. (a) Location of the study area in China; and (b) the digital elecation model (DEM) showing the landslide locations.

resistant formations (limestones) in the anticline core give rise to the formation of narrow mountains (Hu et al., 2009). The Yangtze River meanders through the valley at the core of the Wanxian syncline. As the Yangtze River and its tributaries cross the ridge through water gaps, they converge at almost right angles, creating a lattice-like drainage pattern.

3. Material and methods

3.1. Overall workflow

The study was conducted following these main steps:

(i) Preparation of the landslide inventory: Historical landslides were collected from various sources, and then were divided into three types: reservoir-affected landslide, non-reservoir-affected landslide, and rockfall (type I, II, III).
(ii) Selection of the landslide causal factors: Firstly, 16 landslide influencing factors were chosen, and they were normalized to a range of 0.00–0.99 by using the IV model. Then, the multicollinearity among factors was quantified by the Variance inflation factors and Tolerances. After eliminating factors with collinearity, 15 conditioning factors were set as inputs for LSM.
(iii) Construction of the train and test datasets: Four landslide sample sets (including 733 landslides, 387 landslides I, 231 landslides II, and 115 landslides III, respectively) were used as positive samples, and an equal number of non-landslide samples randomly selected from landslide-free areas as negative samples. Each positive and negative sample set was split into 70% of training and 30% of testing.
(iv) Building the models and generating landslide susceptibility maps: This step can be divided into two parts: the first part involves producing the traditional map using LR, RF, SVM, and DL models with the dataset of all landslides; the second part focuses on generating the susceptibility map that considers landslide typologies. The final susceptibility index is obtained by stacking three susceptibility indexes, each predicted by the best-performing model for different landslide typologies.
(v) Comparing and analyzing the difference between the two maps: We compared the differences between the traditional map and the map considering landslide typologies. To illustrate the reasons for the difference, we analyzed three separate maps (maps of landslides I, landslides II, and landslides III). Fig. 3 illustrates the detailed workflow of this procedure.

3.2. Analysis of landslide inventory

3.2.1. Landslide inventory

Mapping landslide boundaries and constructing a spatial database from the landslide inventory are curial steps in LSM. Currently, ensuring the availability, effectiveness and efficiency, and accuracy of the landslide inventory database is considered a chal-

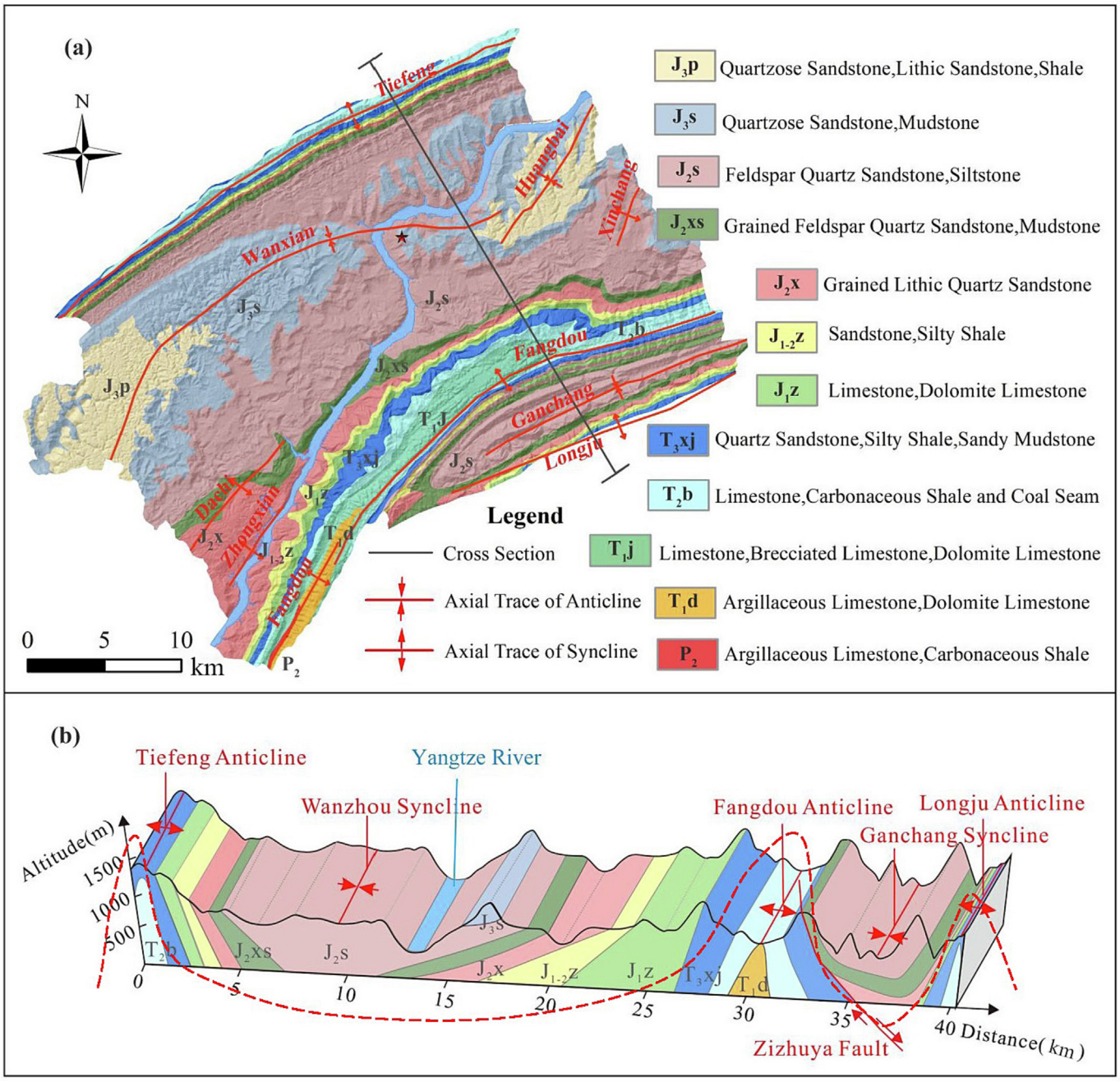

Fig. 2. (a) Geological map; and (b) profile of the study area.

lenging task (Guzzetti et al., 2012). In this case study, the LSM was compiled using various sources, including historical landslide records from the Chongqing Institute of Geological Environment Detection (spanning from 1965 to 2022), geological field investigation lasting for five months (conducted from July 2020 to September 2020 and from October 2021 to November 2021), as well as previous geotechnical reports and literature. During the field survey, we compared, validated and supplemented details of each landslide, such as area, boundary, volume, failure type, triggering event, landslide type, and date of occurrence, among others. Additionally, we updated the information on 50 new landslides in the study area during the heavy rainfall period in July 2020 (with a monthly accumulated rainfall of 440.2 mm). Finally, a total of 733 landslides were mapped as polygons, covering an area of approximately 55×10^6 m^2, representing 12% of the study area. The size of landslide scars varies significantly, ranging from 346 m^2 to 1.407×10^6 m^2. The depth of landslide sliding surfaces range from 0.2 to 42.7 m, and their volumes between 45 m^3 to 2.9×10^7 m^3.

3.2.2. Landslide types

In this study case, 733 landslides were divided into three categories: (i) reservoir-affected landslide, which is caused by drastic changes in hydrological conditions resulting from the periodic fluctuation of the reservoir water; (ii) non-reservoir-affected landslide, induced by torrential rainfall or various human activities; and (iii) rockfalls, which is a geologic process of rapid downward movement of rock and small rock slide (hereinafter called type I, II, III).

A watershed is an area of land that drains rainfall or snowmelt into a specific waterbody, including streams, lakes, rivers, and the

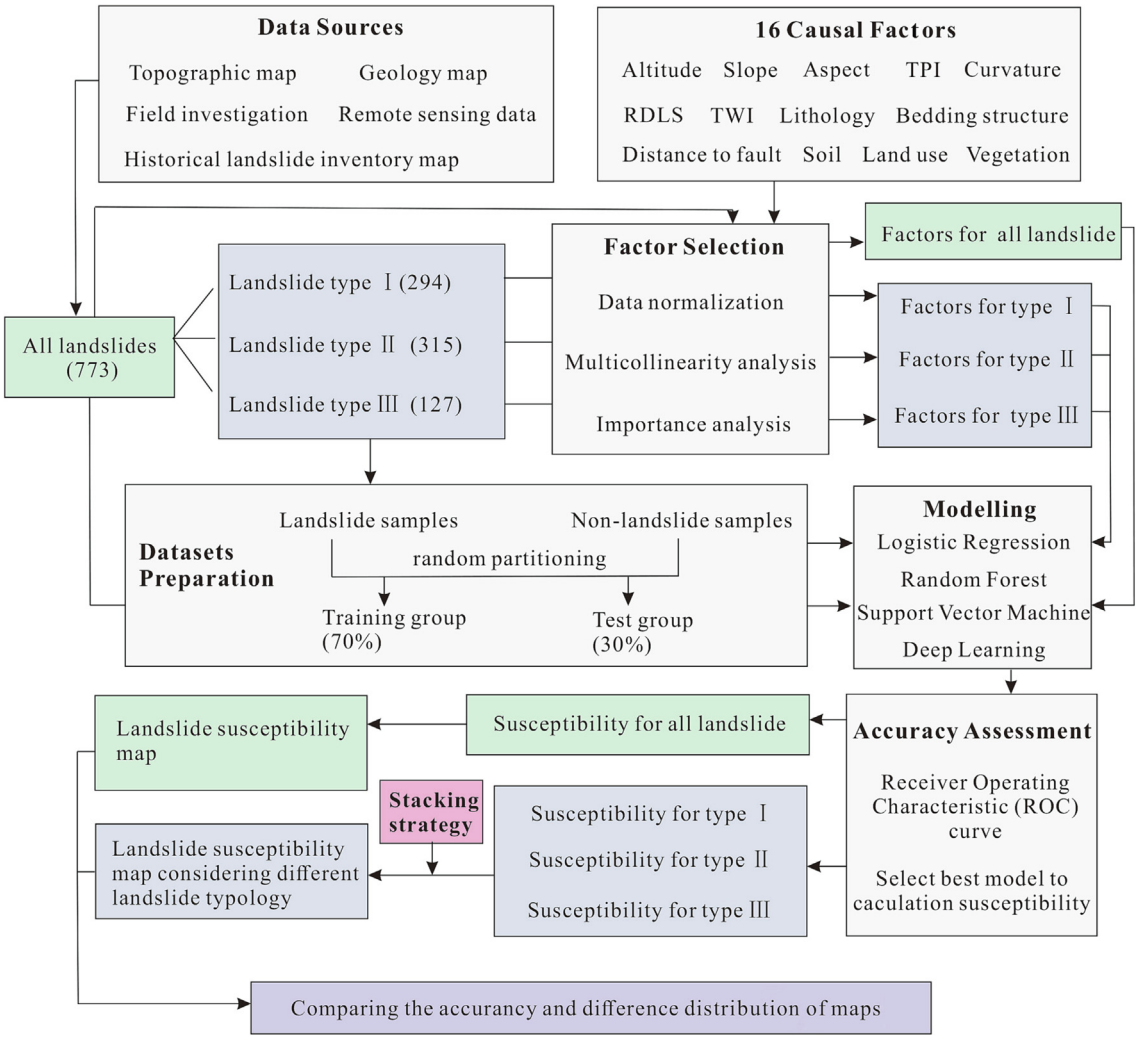

Fig. 3. Workflow of this study.

ocean (Tekin and Çan, 2022). As shown in Fig. 4, it is evident that the hydrogeology of landslides which outside of the Yangtze River's watershed was not affected by the changes in reservoir water level. According to this point of view, 387 landslides within the watershed region were classified as type I, whereas 231 landslides outside were classified as type II. Then, 115 rockfalls and a few rock slides were classified as type III (Fig. 5). The watershed boundaries of the Yangtze River were extracted from DEM data using the Hydrology Analysis Tool of ArcGIS.

In the field investigation, the stability of landslides was categorized into three states: stable, limited stable, and unstable based on recorded deformation signs for each landslide (Table 1). Overall, 24.5% of landslides were found to be stable, showing no signs of deformation. Approximately 54% of landslides were classified as limited stable, indicating that minor disturbances could potentially cause the landslide to be reactive. Meanwhile, 21.5% of landslides were categorized as unstable due to significant deformation, such as new cracks on buildings or the landslide surface, rolling stone

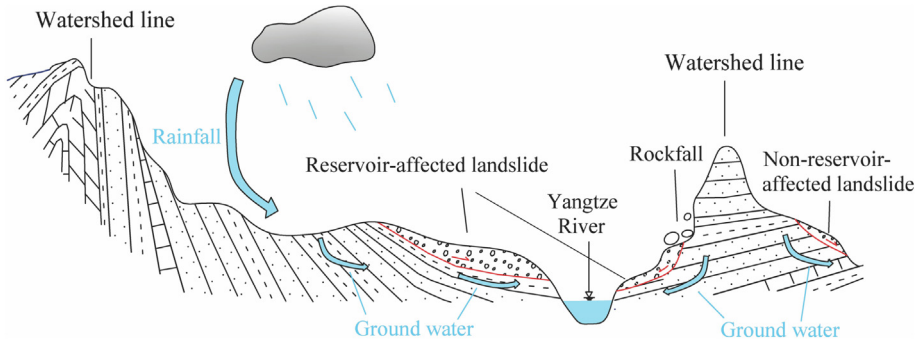

Fig. 4. Reservoir-affected landslides and non-reservoir-affected landslides are divided by the first watershed line.

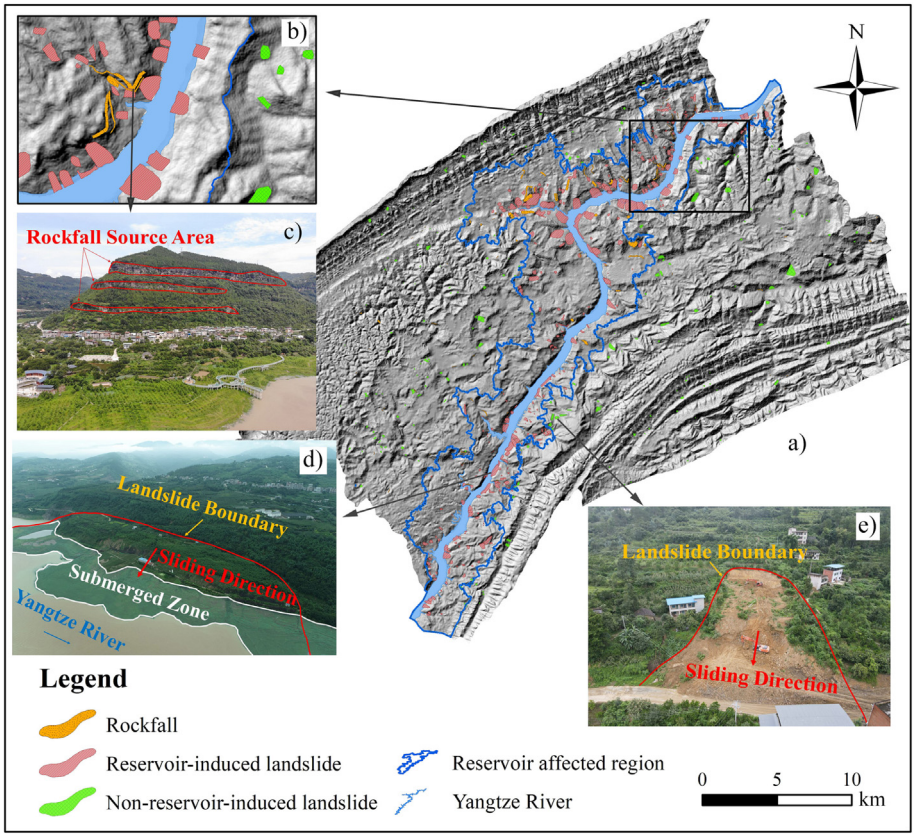

Fig. 5. (a) The study area location; (b) detailed spatial distribution of different types of landslides; (c) rockfall poses a serious threat to residents' safety; (d) the foot of reservoir-affected landslide submerged by water; and (e) non-reservoir-affected landslide caused by road construction.

Table 1
Characteristics of three types landslides.

Characteristics	Category	Number of landslides		
		L. I	*L.* II	*L.* III
Volume ($\times 10^4$ m^3)	Small (<10)	67	91	89
	Medium (10–100)	239	119	26
	Huge (100–1000)	76	21	0
	Extra huge (>1000)	5	0	0
Depth (m)	Shallow (<10)	246	191	/
	Medium (10–25)	130	39	/
	Deep (>25)	11	1	/
State of stability	Stable	96	61	23
	Limited stable	194	128	73
	Unstable	97	42	19

failure, etc. The volume of reservoir-affected landslides is mainly medium and huge (about 61.7% and 19.6%). In contrast, the volume of non-reservoir-affected landslides is smaller, with 51.5% being medium landslides and 39.4% being small landslides. According to the statistics of drilling data and field surveys, most of the deep-seated landslides are reservoir-affected landslides, and the sliding surfaces of those landslides are mainly arc-shaped or linear-shaped. However, about 82.6% of non-reservoir-affected landslides are shallow landslides with a depth of less than 10 m.

Furthermore, the violin plot shows the differences in the size of landslide scars and distance to the Yangtze River among these three types of landslides. As shown in Fig. 6, the area distribution of the type I landslides is relatively scattered, except for several very huge values, which are mainly concentrated at 993 m^2. The area distribution of landslides of type II and III is more concentrated than type I, with values of 725 m^2 and 767 m^2, respectively. Regarding the characteristic distance to the Yangtze River, type II landslides are relatively uniform, mainly concentrated in the range of 4 km to 11.5 km. Landslides of type I and III are mainly concentrated at 0.7 km and 2 km, respectively.

3.3. Landslide causal factors

Landslides are influenced by a series of dynamic and static factors, which are used as the input data for LSM. In various geological settings, dynamic factors mainly include rainfall, earthquake, changes in underground water, etc., while static factors include lithology, faults, landform variations, etc. (Guzzetti et al., 2005). Although there are numerous studies focusing on LSM, there are no universal rules regarding the selection of landslide causal factors (Merghadi et al., 2020). In this study case, we considered the triggering mechanisms of different landslides, and selected 16 factors for LSM, including altitude, slope, aspect, curvature, topographic position index (TPI), degree of relief, topographic wetness

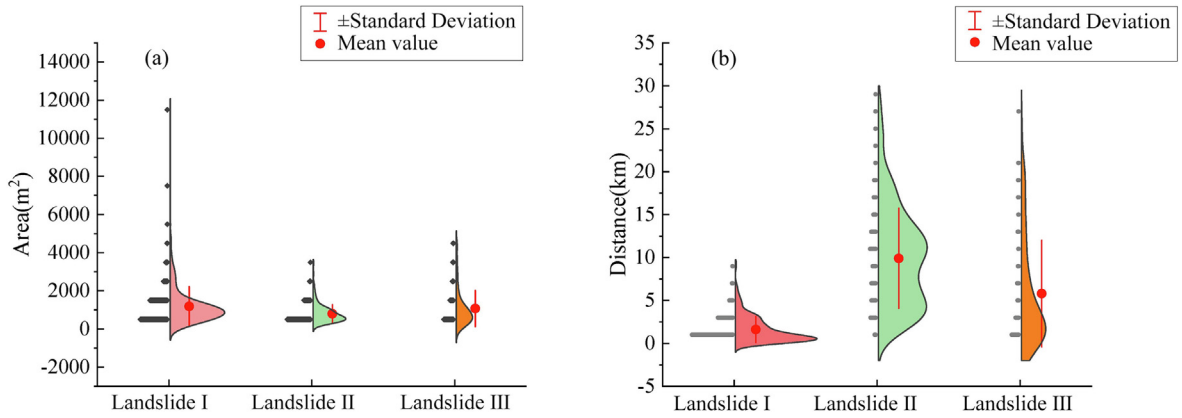

Fig. 6. Spatial distribution characteristics of different types of landslides in the study area: (a) distance from the Yangtze River; and (b) the area of each landslide.

index (TWI), bedding structure (BS), lithology, soils, distance to Yangtze River, distance to streams, distance to faults, distance to roads, land use, and vegetation (Fig. 7). Table 2 outlines the data source of these 16 causal factors. In addition, rainfall is main factor changing the water balance on hillslopes and affecting slope stability in the TGRA. Unfortunately, the collected rainfall data have low resolution and cannot provide detailed and accurate data for LSM in this study.

Many literatures have shown that topographic factors play a primary role in LSM, and the maps of these factors are usually derived from the digital elevation model (DEM) (Dai et al., 2002). In this study, we obtained a 25 m × 25 m resolution DEM from a topographic map, and selected seven topographical factors (altitude, slope, aspect, curvature, TPI, degree of relief, SPI and TWI) for conducting LSM. Lithology, BS, and soils are static factors related to the material basis of landslides, and we obtained them from the geological map and soil map of the region. The lithology units were classified into twelve groups based on the age of deposition. BS reflect the attitudes of the slope aspect and rock layer (Yu et al., 2022), and it was divided into five categories: anaclinal slope (BS1), anaclinal oblique slope (BS2), dip slope (BS3), dip slope (BS4), and transverse slope (BS5). According to the field investigation and extensive literature (Zhou et al., 2018), the potentially impacted distance of trains, national highways, and other roads, were set at 1000 m, 500 m, and 200 m, respectively. The potential impacted distances of the Yangtze River and streams were set at 1000 m, and 500 m, respectively. Distance maps of faults, Yangtze River, streams, and roads were produced using the Euclidean distance analysis tool in ArcGIS 10.6.

3.4. Factor normalization

In LSM, feature normalization is useful in reducing overfitting and improving model performance (Yu et al., 2022). The normalization process used in this study consists of two parts: (i) for continuous factors (e.g., altitude, slope, etc.), each factor was classified into a suitable number of sub-classes on average. Then, sub-classes with similar IV were recombined into new classes; (ii) for factors with categorical and nominal data (e.g., lithology, soil, etc.), the value of each category was directly calculated using the IV model. Finally, all landslide conditional factors were normalized between 0.01 and 0.99, as shown in Supplementary Data (Table S1).

3.5. Landslide susceptibility models

3.5.1. Information value

The Information Value (IV) model is a statistical model proposed by Yin (1990), and IV is a fundamental concept in information theory that measures the amount of information carried by an event or message. The IV model is commonly used in predicting slope stability, landslide susceptibility, and quantifying the correlation between landslide occurrence and its conditional factors. In this study, the IV model was used to quantify the value of each category of landslide causal factors.

3.5.2. Logistic regression

Logistic Regression (LR) is a generalized linear algorithm from the field of statistics used to solve binary classification problems (Erener et al., 2016). The LR model is the most frequently used model in LSM because it is computationally efficient and can effectively describe the linear relationship between landslide occurrences and multiple conditioning factors. In essence, LR connects the occurrence (1) or absence (0) of landslides to a logistic function with the landslide causal factors, and the function can be expressed as:

$$y(x) = \frac{1}{1 + e^{-\theta^T x}} \quad (1)$$

where, the independent variable y refers to the occurrence probability of landslides, and the independent variable x refers to the landslide conditional factors.

3.5.3. Random forest

The Random Forest (RF) model is a nonlinear ensemble ML model based on multiple weak learners (Decision Trees) (Dou et al., 2019). It has been widely applied in various fields, including classification, regression, feature selection, and anomaly detection. When solving classification problems, the RF model aggregates the class predictions of the training samples by voting from each tree's predicted class. Numerous studies have demonstrated that RF is a powerful and flexible tool for generating landslide susceptibility maps, achieving accuracies of over 90% in different geological environments (Hong et al., 2016; Dou et al., 2019). The main advantage of the RF model is its ability to effectively reduce overfitting, and demonstrate robustness to missing data, imbalanced data and outliers.

3.5.4. Support vector machine

Support Vector Machine (SVM) is a supervised ML model extensively used for classification and regression tasks (Marjanović et al., 2011). Its primary aim is to find an optimal hyperplane that maximally separates different classes in the feature space. Compared with the RF model, the SVM model performs well in capturing linear or nonlinear relationships between features, even when dealing with small datasets (Merghadi et al., 2020). However, the SVM often requires significant computational resources, and can

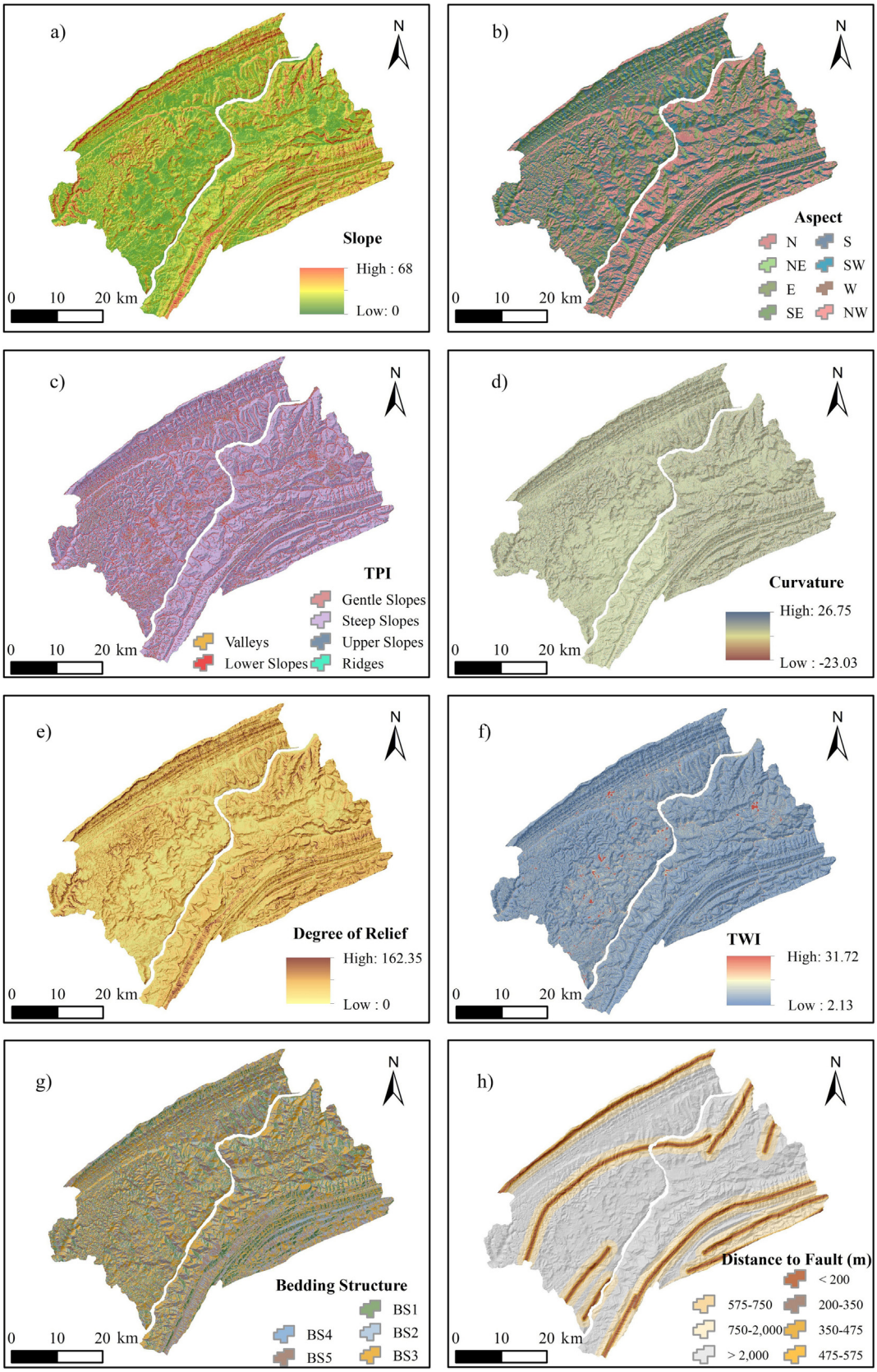

Fig. 7. Landslide causal factors of the study area: (a) slope, (b) aspect, (c) TPI, (d) curvature, (e) degree of relief, (f) TWI, (g) bedding structure, (h) distance to faults, (i) distance to Yangtze River, (j) distance to stream and (k) distance to road. (l) land use, (m) soil, and (n) vegetation.

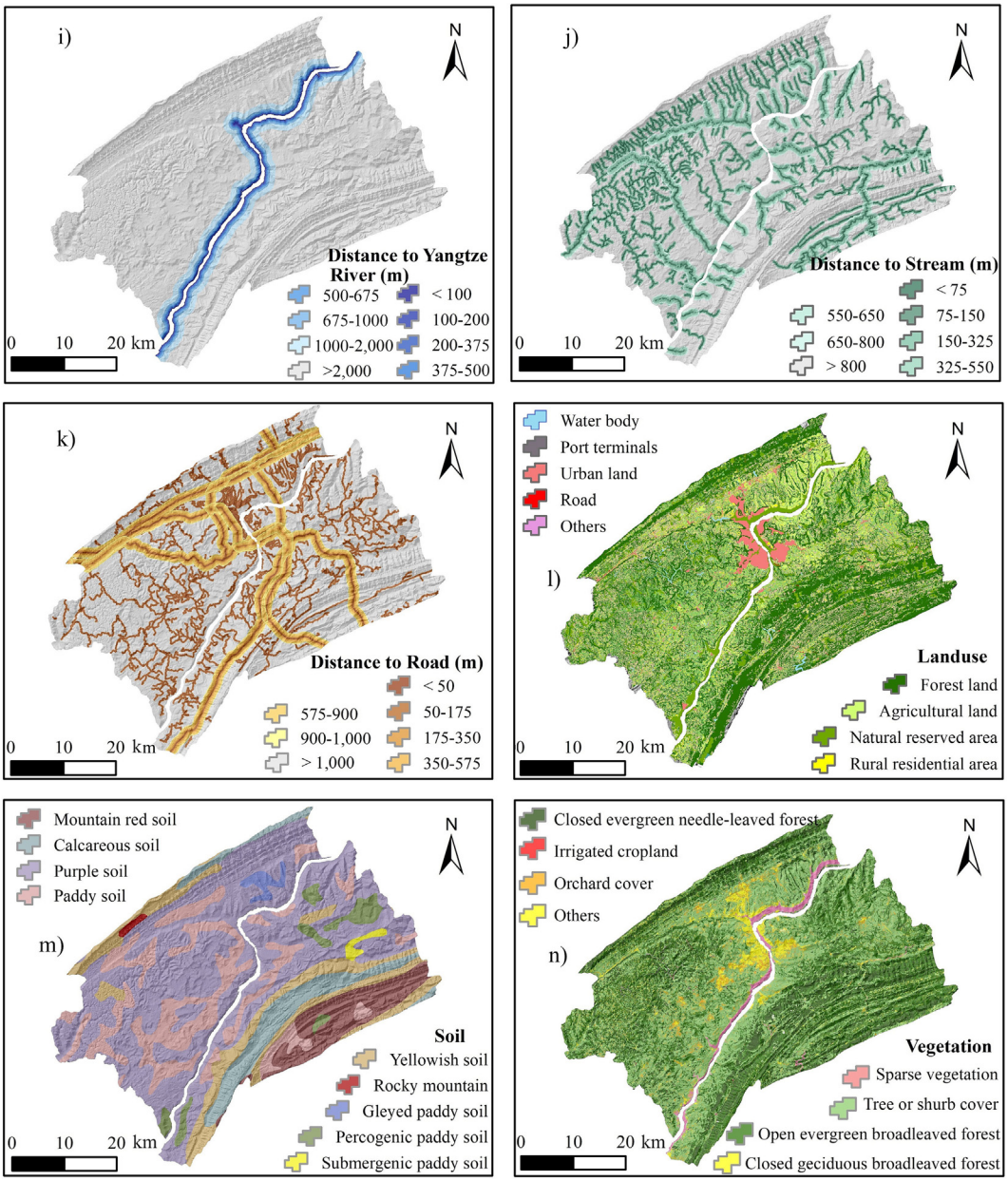

Fig. 7 (*continued*)

Table 2
Data sources for landslide causal factors.

Input data	Data source	Data type	Resolution (scale)	Causal factors
Topographic map (DEM)	Obtained from the Chongqing Institute of Geological Environment Detection (CIGED) (http://www.caghp.org/standard.php)	Polygon	1:10,000 (25 m × 25 m)	Altitude, slope, aspect, curvature, TPI, degree of relief, SPI and TWI
Geological map	Obtained from CIGED and field survey	Polygon	1:50,000	Lithology Bedding structure Distance to faults Distance to streams
Land use map	Obtained from CIGED	Polygon	1:10,000	Land use Distance to roads Distance to Yangtze River
Soil map	China Resource and Environment Science and Data Center (https://www.resdc.cn/data.aspx?DATAID=145)	Polygon	1:1,000,000	Soils
Remote sensing map	Derived from the Sentinel-2A on the Google Earth Engine	Grid	25 m × 25 m	Vegetation

be sensitive to parameter tuning. The performance of the SVM model mainly depends on the kernel function options ('linear', 'polynomial', 'radial basis function (RBF)', and 'sigmoid') and other hyper-parameters ('C, penalty function or regularization parameter', 'Gamma, the kernel coefficient', and so on). In this study case, the grid-based search method was utilized for tuning the models.

3.5.5. Deep learning model

In this study, we selected residual learning network (ResNet-18), a typical CNN architecture proposed by Kaiming He in 2015 (He et al., 2016), to conduct LSM. ResNet-18 is composed of residual building blocks, and the structure of a residual building block is shown in Fig. 8a. In the residual building block, the final output is the sum of two parts: one part is the input data X directly output without any operation, which is named a shortcut connection or skip connection; the other part is the fitting output by the stacked convolution layers.

In the process of residual learning, the skip connection does not have any parameters, and increasing the number of residual blocks does not add too much additional parameter burden to the model. As a result, ResNet can easily improve performance by considerably increasing the depth, and are wieldy used for the landslide detection and susceptibility modelling (Liu et al., 2021; Aslam et al., 2023).

3.5.6. Stacking method

Stacking is an ensemble learning technique that combines the predictions of multiple individual base learners to form a stronger and more accurate generalization model. It was proposed by Smyth and Wolpert (1999), and consisted of two key steps (Fig. 9): the first step is the basic learning step, and the second step is the meta-learning step. In the first step, each individual base-classifier is trained to generate predictions. In the second step, the meta-classifier is used to combine the base models' predictions and generate the final prediction. Increasing the number of base models can theoretically enhance the stacking model's performance by capturing different data features. However, adding redundant models may not provide additional benefits and could lead to overfitting. In this study case, the basic-classifiers of the stacking framework were LR, RF, SVM and DL model, while the meta-classifier was LR.

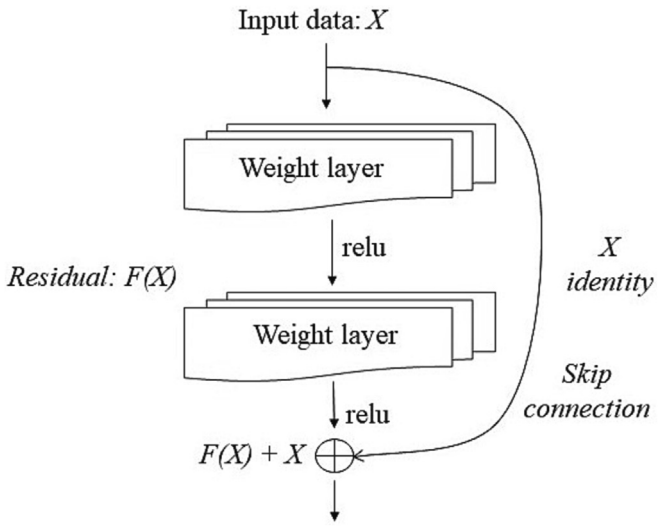

Fig. 8. Residual learning: a building block.

3.6. Accuracy assessment

Since LSM is a binary classification task, the Receiver Operating Characteristic (ROC) curve and Area Under the Curve (AUC) are used to validate the performance of the models in this study (Merghadi et al., 2020). The ROC curve reflects the relationship between the True Positive Rate (TPR) and False Positive Rate (FPR) at various threshold settings. The closer the ROC curve is to the top-left corner, the better the model's performance. AUC is calculated from the ROC curve, and used to quantify the overall performance of the models. The AUC value ranges from 0 to 1, where a higher value indicates better discrimination and a more accurate model. According to the study by Sreenivas and Venkataratnam in 2006, AUC can be divided into five levels: Poor (0.5–0.6), Average (0.6–0.7), Good (0.7–0.8), Very Good (0.8–0.9), and Excellent (0.9–1).

4. Results

4.1. Analysis of causal factors

4.1.1. Multicollinearity analysis

In the database of landslide causal factors, it is common to observe a phenomenon where certain factors have a strong correlation with each other, especially in topographic factors (Yu et al., 2022). This multicollinearity can often lead to a reduction in the model's performance. To address this issue, we use statistical measures such as Variance inflation factors (VIF) and Tolerance to detect and quantify the extent of multicollinearity in the landslide causal factors. VIF is an index that measures how much the variance of the estimated regression coefficient is inflated due to multicollinearity (Lin et al., 2011). The VIF for the predictor variable x_j can be computed as follows:

$$VIF = \frac{1}{1 - R^2_{x_j|x_{-j}}} \tag{2}$$

where, $1 - R^2_{x_j|x_{-j}}$ represents the coefficient of determination (R-squared) from the regression model of x_j on the remaining predictor variables.

Tolerance is the reciprocal of VIF and provides an alternative perspective on multicollinearity. Typically, when VIF $\geq$ 5 or tolerance $\leq$ 0.2, it indicates that the factors have a multicollinearity (Lin et al., 2011). In this study case, based on four landslide inventory datasets, the multicollinearity analysis of 16 landslide causal factors was developed by SPSS software (Table 3). The result indicated that Slope is collinear with RDLS. After remove RDLS, there is no collinearity among the remained 15 factors.

4.1.2. Comparative importance analysis of different landslide types

Quantifying feature importance is valuable for identifying the most influential variables in landslide occurrence, understanding the underlying relationships among landslide causal factors, and building interpretable susceptibility models (Reichenbach et al., 2018). RF can provide feature importance rankings, which are quantified by aggregating the impurity decrease (usually measured using the Gini impurity or information gain) caused by each feature across all decision trees in the forest (Yu et al., 2022).

Therefore, the feature importance values of the 15 landslide predisposing factors were computed using the attribute "*feature_importance*" of the RF model in Anaconda software. Higher values for a factor indicate a greater influence on landslides. The results showed that the 15 influencing factors had different impacts on different types of landslides in the study area (Table 4). The two most significant contributing factors for the landslide inventory datasets of all landslides, reservoir-affected landslides,

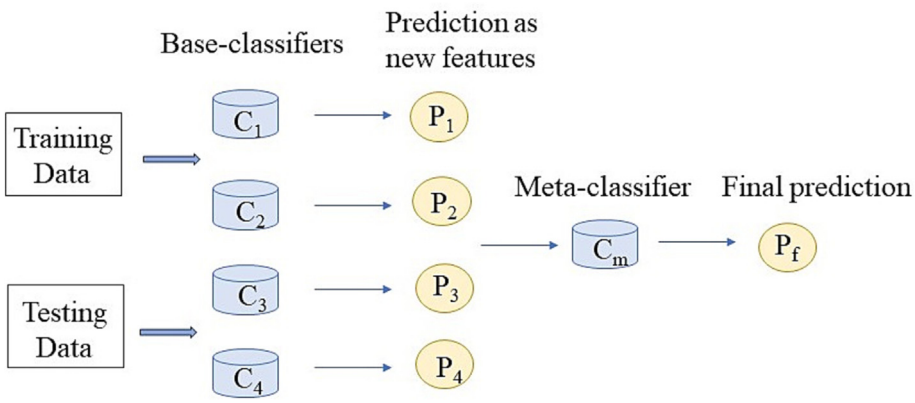

Fig. 9. The structure of Stacking method.

Table 3
The tolerances and VIF of causal factors.

Factor	All landslides		Non-reservoir-affected landslides		Reservoir-affected landslides		Rockfalls	
	Tolerances	VIF	Tolerances	VIF	Tolerances	VIF	Tolerances	VIF
Altitude	0.533	1.875	0.566	1.767	0.554	1.806	0.581	1.720
Slope	**0.192**	**5.207**	**0.193**	**5.193**	**0.192**	**5.202**	**0.192**	**5.197**
Aspect	0.868	1.152	0.879	1.138	0.868	1.151	0.829	1.206
TPI	0.802	1.247	0.799	1.046	0.815	1.227	0.715	1.399
Curvature	0.893	1.119	0.890	1.123	0.895	1.117	0.908	1.101
RDLS	**0.187**	**5.361**	**0.188**	**5.317**	**0.186**	**5.375**	**0.189**	**5.294**
TWI	0.628	1.591	0.695	1.439	0.638	1.568	0.636	1.571
Lithology	0.706	1.416	0.973	1.027	0.713	1.402	0.776	1.289
BS	0.994	1.006	0.923	1.083	0.981	1.020	0.866	1.154
Fault	0.777	1.287	0.826	1.211	0.844	1.185	0.750	1.333
Yangtze	0.657	1.522	0.619	1.616	0.734	1.363	0.813	1.229
Stream	0.928	1.078	0.840	1.190	0.942	1.061	0.945	1.058
Road	0.875	1.142	0.956	1.046	0.879	1.137	0.864	1.158
Land use	0.670	1.494	0.883	1.132	0.680	1.471	0.777	1.288
Soil	0.574	1.742	0.935	1.027	0.561	1.781	0.676	1.480
Vegetation	0.376	2.658	0.651	1.535	0.368	2.720	0.499	2.004

Table 4
The important value of causal factors.

Factor	All landslides	Non-reservoir-affected landslides	Reservoir-affected landslides	Rockfalls
Altitude	0.097	**0.148**	**0.235**	**0.238**
Slope	0.027	0.094	0.032	**0.122**
Aspect	0.026	0.061	0.034	0.030
TPI	0.034	0.052	0.030	0.019
Curvature	0.021	0.063	0.025	0.037
TWI	0.021	0.066	0.026	0.046
Lithology	**0.190**	**0.096**	0.023	0.120
BS	0.025	0.041	0.029	0.021
Fault	0.051	0.044	0.030	0.029
Yangtze	**0.132**	0.058	**0.237**	0.035
Stream	0.126	0.059	0.034	0.053
Road	0.048	0.066	0.045	0.058
Land use	0.050	0.047	0.079	0.037
Soil	0.090	0.070	0.071	0.054
Vegetation	0.060	0.035	0.072	0.100

non-reservoir-affected landslides, and rockfall were Lithology and Distance to Yangtze River with values of 0.190, and 0.132, Altitude and Distance to Yangtze River with values of 0.235, and 0.237, Altitude and Lithology with values of 0.148, and 0.096, and Altitude and Slope values of 0.238, 0.122, respectively.

4.2. Landslide susceptibility modelling

First, we created four training and testing datasets, each consisting of inventory events for all landslides, reservoir-affected landslides, non-reservoir-affected landslides, and rockfalls. Each dataset was split with 70% landslide samples for training and the remaining 30% for testing, and its distribution was shown in Fig. 10. Simultaneously, an equal number of non-landslide samples were randomly selected from the landslide-free zone to balance the dataset.

When the data distribution in both the training and testing sets is similar, the assessment outcomes of a model can more precisely indicate its performance in practical applications (Zhou et al., 2022a, 2022b; Qiu and Zhou, 2023a, 2023b). The train and test datasets, which cover all types of landslide samples, were used to conduct the distribution analysis in this study. As shown in Fig. 11, violin plots were employed to display the distribution of continuous factors, and frequency distribution histograms were utilized for discrete factors. It can be seen that the distribution of the training and testing datasets is mainly consistent, ensuring the reliability of the model testing.

Secondly, four models, namely LR, RF, SVM, and DL, were constructed to compute the landslide susceptibility index. In the training process, the three ML models were built using the scikit-learn library (Sklearn) in Anaconda software, and the best hyper-

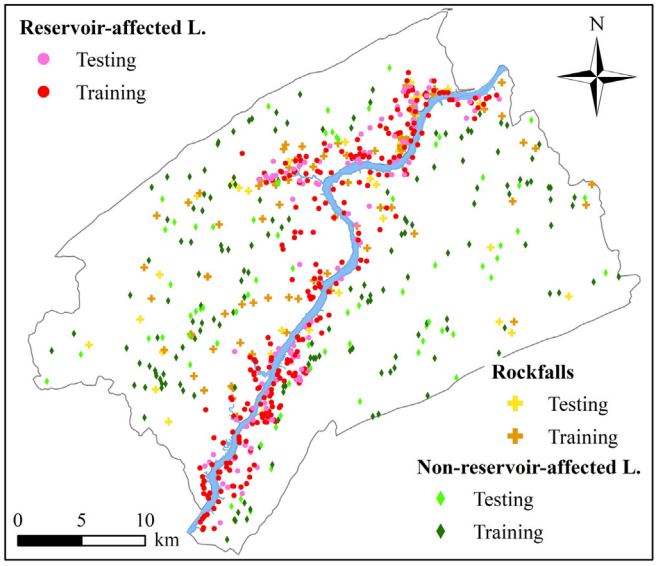

Fig. 10. The distribution of all types' landslides in training and testing datasets.

parameters for these models were tuned by the "Grid-SearchCV" module in Sklearn (Table 5). The DL model used in this study, ResNet-18, is composed of four residual blocks, each containing two convolutional layers with a kernel size of 1 × 3. After the residual blocks, a global average pooling layer computes the average value of each input feature (where is 1 × number of landslide causal factors × 1). The output of the global average pooling layer is then fed into a fully connected layer with a Softmax activation function for the final two classifications (where is landslide: 1, non-landslide: 0). Several related parameters were set up: the batch size is 64, the number of epochs is 100, and the dropout rate is 0.2.

After training, the AUC was used to compare the performance of the four models, and the best model for reservoir-affected landslides, non-reservoir-affected landslides, and rockfalls were selected as the basic learner for the Stacking framework. Table 6 lists the AUC of all models, and Fig. 10 shows the ROC curve of the train and test datasets. The DL model achieved excellent performance in all landslides, reservoir-affected landslides and rockfalls, with AUC of training and testing are 0.922 and 0.854, 0.956 and 0.919, 0.968 and 0.855, respectively. The RF model outperformed the other models for non-reservoir-affected landslides, with AUC values of 0.867 for training and 0.720 for testing (see Fig. 13).

Finally, the susceptibility indexes of reservoir-affected landslides, non-reservoir-affected landslides, and rockfalls were used as input data, and the final susceptibility index was calculated using the Stacking method, with the highest AUC values of 0.966 for training and 0.880 for testing (Table 6).

4.3. Landslide susceptibility maps

For clear interpretation and analysis purposes, the landslide susceptibility indexes of models are classified into five categories: Very High (10%), High (20%), Moderate (20%), Low (20%) and Non-susceptibility (30%). Consequently, this study generated a total of five maps (Fig. 11).

5. Discussion

An accurate landslide susceptibility map plays a pivotal role in mitigating geological disasters, reducing human and economic losses, and enhancing land use efficiency in mountainous regions (Guzzetti et al., 2020). Although numerous methodologies for LSM have been developed, especially with the exploration of ML and DL algorithms, few approaches consider the impact of landslide types on LSM. In this study, new ensemble frameworks were proposed to generate the landslide susceptibility map, considering landslide types. Hence, in this discussion section, we focus on: (i) major factors of different types of landslides, (ii) model performance comparison and analysis, and (iii) the spatial distribution of difference between different maps.

5.1. Importance analysis of causal factors

Due to significant differences in predisposing events, failure mechanisms, and displacement mechanisms, the same factor can have varying impacts on the occurrence of different types of landslides in an area (Loche et al., 2022). In this study case, the importance value of 15 landslide causal factors was quantified using the RF model, and the relationships between different categories of each factor and landslides were computed using the IV model. Among these 15 factors, Altitude, Lithology, Slope, and Distance to Yangtze River play vital roles in the LSM. The details of these four factors are discussion as follows.

In this study, altitude has proven to be crucial for all types of landslides, with IV values of 0.238 for rockfalls, 0.235 for reservoir-affected landslides, and 0.148 for non-reservoir-affected landslides, respectively. Although the importance of factors can vary depending on the local setting and geological conditions, many previous studies have also proven the effectiveness of altitude in LSM (Marchesini et al., 2014; Budimir et al., 2015). Therefore, it is essential to obtain high-quality DEM data and utilize detailed morphometric factors when conducting LSM for any type of landslides. Furthermore, the IV model reveals that the importance of different altitude subcategories varies significantly between the three types of landslides. The most important subcategories for reservoir-affected landslides, rockfalls, and non-reservoir-affected landslides are [50 m, 170 m], [170 m, 300 m], and [300 m, 430 m], with IV values of 2.235, 1.073, 0.439, respectively. This finding aligns with the field investigation in our study, which revealed that the foot of reservoir-affected landslides is mainly located at altitudes between 120 m and 170 m, where the Yangtze River's intense erosion occurs (Tang et al., 2019). Simultaneously, rockfalls are usually distributed within the elevation range of 170 to 300 m and, together with the reservoir-affected landslide, exhibit a composite chain-like characteristic of "falling or toppling above, and sliding below".

Lithology is the most important for all landslides, the second most important for non-reservoir-affected landslides, and the third most important for rockfalls, with importance values of 0.19, 0.096, and 0.12, respectively. However, it has minimal importance for reservoir-affected landslides, with an importance value of only 0.023. This result is unusual, but reasonable. According to the statistics in Supplementary Data (Table S1), 78.15% of the study area is covered by $J_{2\text{-}3}$ lithology, and 93.83% of reservoir-affected landslides occurred in the bedrock of $J_{2\text{-}3}$. From this perspective, the reason may be that the age of the formation may not provide enough information to conduct LSM for reservoir-affected landslides. More detailed geological information, such as lithological classification and structural units, is needed for LSM. Similar to the previous findings of Segoni et al. (2020), which explored the performance of six parameters involving different geological information in LSM, this work emphasizes the importance of utilizing as much geological information as possible, regardless of its accuracy or scale.

Distance to Yangtze River is the most important factor for reservoir-affected landslides, with an importance value of 0.237.

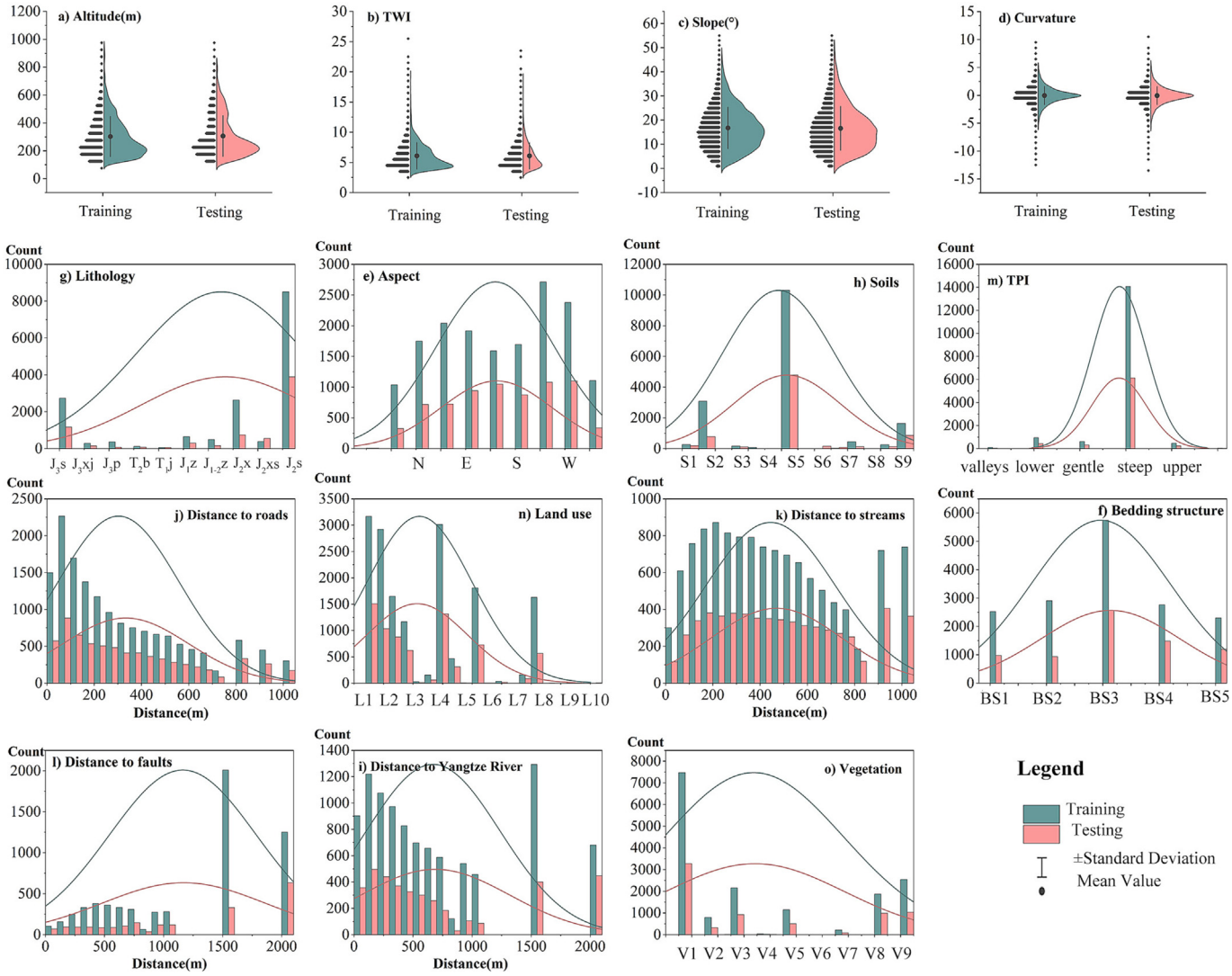

Fig. 11. Comparison of training and testing datasets distribution.

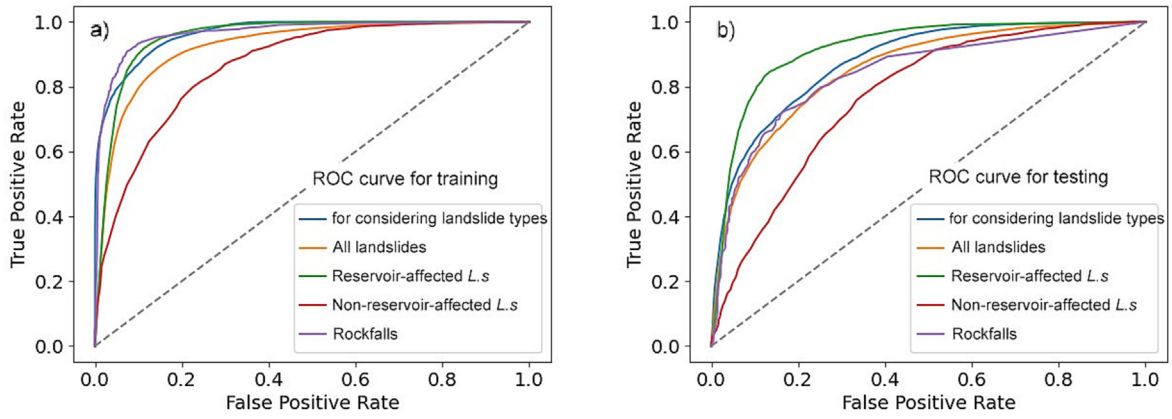

Fig. 12. The ROC curves for landslide susceptibility assessment: (a) training and (b) testing.

However, it is less important for other types of landslides (0.094 for non-reservoir-affected landslides and 0.032 for rockfalls). It is evident that the rockfalls occur in high-slope terrain in the study area, and the IV model shows that the slope categories within [42.5°, 68°], [6.5°, 15°], [25.5°, 32°] the most important for rockfalls, reservoir-affected landslides, and non-reservoir-affected landslides, with IV values of 1.073, 0.210, 0.117, respectively. Altitude and distance to Yangtze River were the two most important factors for reservoir-affected landslides, and the importance values of related factors were less than 0.08. This result indicates that these two factors significantly impact the occurrence of reservoir-affected landslides.

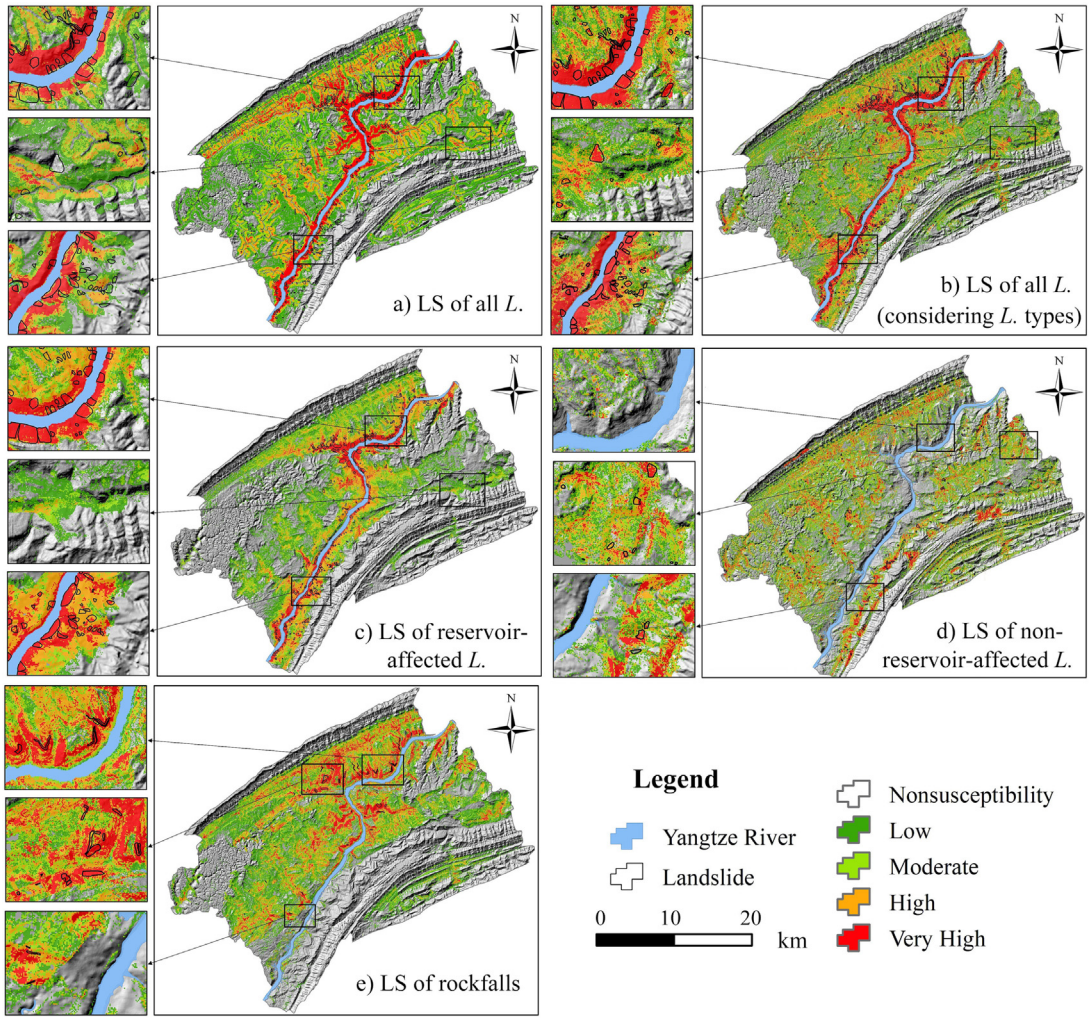

Fig. 13. Landslides susceptibility maps of: (a) all landslides, (b) all landslides considering landslide types, (c) reservoir-affected landslides, (d) non-reservoir-affected landslides, and (e) rockfalls.

Table 5
Optimized parameters of five models and search spaces.

Model	Parameters	Search space	Best value (grid search with 5-fold cross validation)
LR	C	$[10^{-3}–10^{3}]$	0.1
	Solver	Newton-cg, lbfgs, liblinear, sag	Liblinear
RF	Number of base estimators	[10–500]	130
	Maximum tree depth	[2–20]	17
SVM	Kernel function	Linear, RBF, Sigmoid	RBF
	C	$[10^{-3}–10^{3}]$	5
	Gamma	$[10^{-3}–10^{3}]$	0.3
DL	Loss function	Cross-entropy loss	Cross-entropy loss
	Active function	ReLU, Tanh, Sigmoid, Linear	ReLU
	Optimization algorithms	Stochastic Gradient Descent (SGD), Root Mean Square Propagation (RMSProp), Adaptive Moment Optimization (Adam)	Adam
	Learning rate	$[10^{-5}–1.0]$	0.3

5.2. Model validation and comparison

Recently, with the rapid development of computation, more attention has been focused on exploring ensemble methods and ML techniques in LSM. Many previous studies have shown that ensemble methods outperform other typical ML models in various geological settings, effectively capturing the nonlinear relationship between landslide causal factors and landslide occurrence (Dou et al., 2020). However, most of the research has compared ensemble frameworks that integrate different base classifiers with other

Table 6
The AUC of the models during the training and testing process.

Landslide types		LR	RF	SVM	DL	Staking	
All landslides	Train	0.780	0.858	0.853	0.922	0.966	
	Test	0.796	0.805	0.665	0.854	0.880	
Reservoir-affected landslides	Train	0.869	0.863	0.886	0.956		
	Test	0.858	0.853	0.861	0.919		
Non-Reservoir-affected landslides	Train	0.664	0.867	0.678	0.939		
	Test	0.570	0.720	0.574	0.616		
Rockfalls	Train	0.843	0.932	0.850	0.968		
	Test	0.833	0.815	0.831	0.855		

ML models. There is currently no study that effectively combines susceptibility zonation for different landslide types based on ensemble strategy.

In this study, three ML models (LR, RF, SVM), and a DL model (Resnet-18) were used to conduct LSM, and then the best models for different types of landslides were selected as the basic learner for Stacking methods. The AUC results showed that DL model outperformed other typical ML algorithms in modelling all landslides, reservoir-affected landslides and rockfalls, with improvements of 0.036 to 0.121 for training and 0.022 to 0.189 for testing. This finding is consistent with several recent studies, which also demonstrated that DL models can achieve advanced predictive ability in LSM when hyper-parameters are suitably tuned and built with high quality and sufficient training samples (Youssef et al., 2022; Yuan and Chen, 2022). In the modelling progress of non-reservoir-affected landslides, the RF model showed the best performance with an ROC of 0.867 for training and 0.720 for testing. Therefore, the DL model was considered as superior tool to map the landslide susceptibility in this study. Overall, when compared with directly modelling all landslides using the DL model, the Stacking method increased the AUC by 0.044 for training and 0.026 for testing. Although the improvement may appear modest, Fig. 11b clearly demonstrates that considering different types of landslides led to more accurate predictions of landslides located away from the Yangtze River. The confusion matrix is a table used to evaluate the performance of classification models, aiding in detecting model bias and variance and uncovering model weaknesses to support subsequent enhancements (Zhou et al., 2022a, 2022b). Therefore, we validated the susceptibility results from the DL and Stacking models using three performance evaluation indices: Recall, Precision, and F1 score (Fig. 14). The results show that the Stacking model performed better than the DL model in Recall, Precision and F1 score.

In addition, we gathered data from several previous studies on LSM conducted in similar geo-environmental regions. These studies by Xiao et al. (2019), Zhang et al. (2016), and Guo et al. (2019) reported AUC values of 0.801 (RF model), 0.73 (K-means model), and 0.808 (weights of evidence model), respectively. Hence, it is reasonable to conclude that LSM considering types of landslides in our study was advised a powerful strategy to generate a high-quality landslide susceptibility map.

5.3. Comparison of landslide susceptibility maps

In landslide susceptibility research, most scientists typically focus on comparing different models in the same area based on

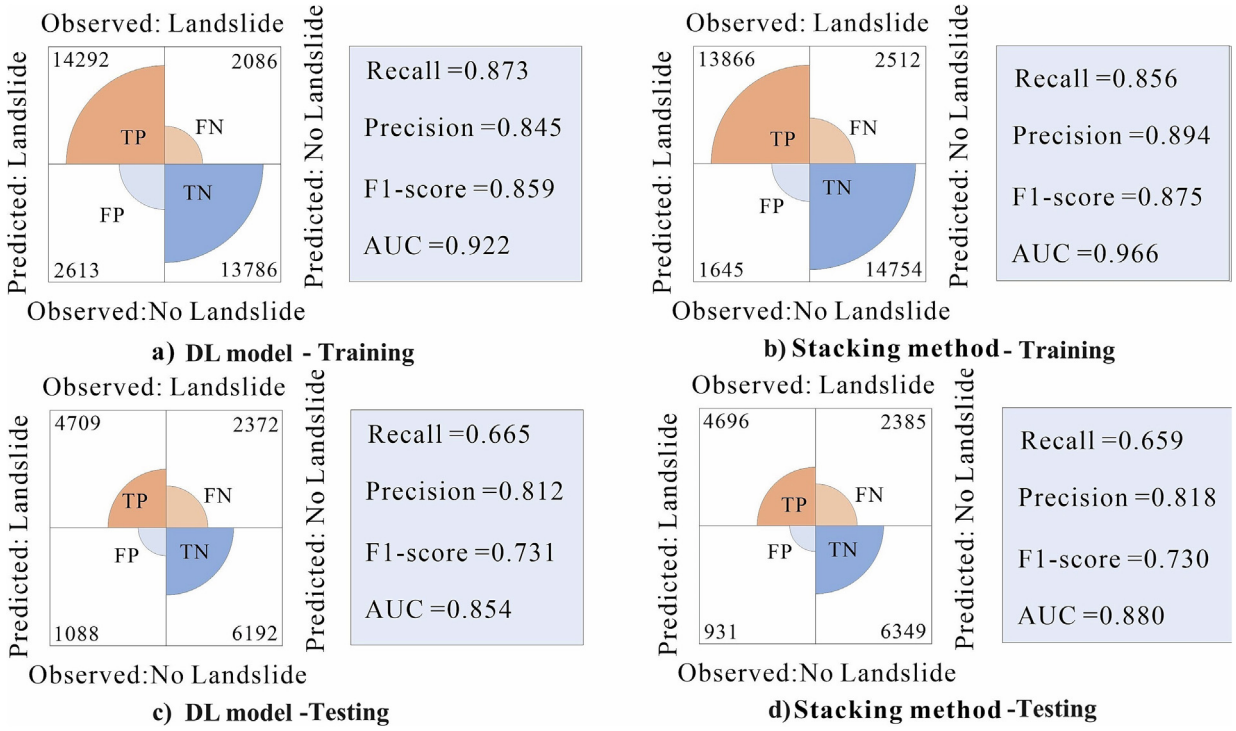

Fig. 14. Confusion matrix results of (a) DL model of training, (b) Stacking method of training, (c) DL model of testing, and (d) Stacking method of testing, respectively.

AUC, OOBE (out of bag error), or a set of indices from the confusion matrix (including recall, sensitivity, specificity, and so on) (Reichenbach et al., 2018). Although these quantified indices can easily and directly indicate which model performs better, there may still be some differences in the spatial distribution pattern of two maps with similar AUC values (Xiao et al., 2020). Therefore, after combining the landslide susceptibility from the three types of landslides, it is necessary to visually inspect the different type's landslides, and further explore whether the differences between these maps are randomly and uniformly distributed or follow some regular spatial patterns.

In this study, we believe that the landslide susceptibility map calculated by the Stacking method was the most accurate map with the largest AUC value. This map was selected as the benchmark (abbreviated as the final map hereafter), while the other four maps were treated as the maps to be tested. Since landslide susceptibility represents the probability of where a landslide is likely to occur (with values between 0 and 1), the difference between the LSI of the map to be tested and the LSI of the benchmark map was defined as their difference (with values ranging from −1 to 1). When the LSI of the benchmark map, we consider it to be underestimated, shown with red color. Conversely, if it is overestimated, it is shown with blue color.

To better investigate the differences between these maps, the value of the difference was divided into several levels: severely underestimated (<−0.6), moderately underestimated (−0.6 to −0.3), mildly underestimated (−0.3 to −0.1), approximate (−0.1 to 0.1), mildly overestimated (0.1–0.3), moderately overestimated (0.3–0.6), severely overestimated (>0.6). Finally, four comparison maps were generated using the raster calculation tool in ArcGIS (Fig. 15).

It is evident that the overestimation and underestimation points in these four comparison maps are not evenly distributed and show distinct orientations. In the comparison between the final map, considering landslide types, and the original map without landslide types, the overestimation points are mainly located in the area after the first watershed with the Yangtze River, and the two small valleys on the north part of the study area; while the underestimated points are situated in the hill area with elevations of 700–800 m (Fig. 15a). In the comparison of the reservoir-affected landslides susceptibility map and the final map, the overestimation points are concentrated on the slopes where non-reservoir-affected landslides occur, while there are few underestimation points, which are distributed in the reservoir slopes (Fig. 15b). In the comparison of the non-reservoir-affected landslides susceptibility map and the final map, the difference level is mainly several overestimated points, and the overestimation points are concentrated on both sides of the Yangtze River (Fig. 15c). In the comparison of the rockfalls susceptibility map and the final map, a significant number of overestimated points

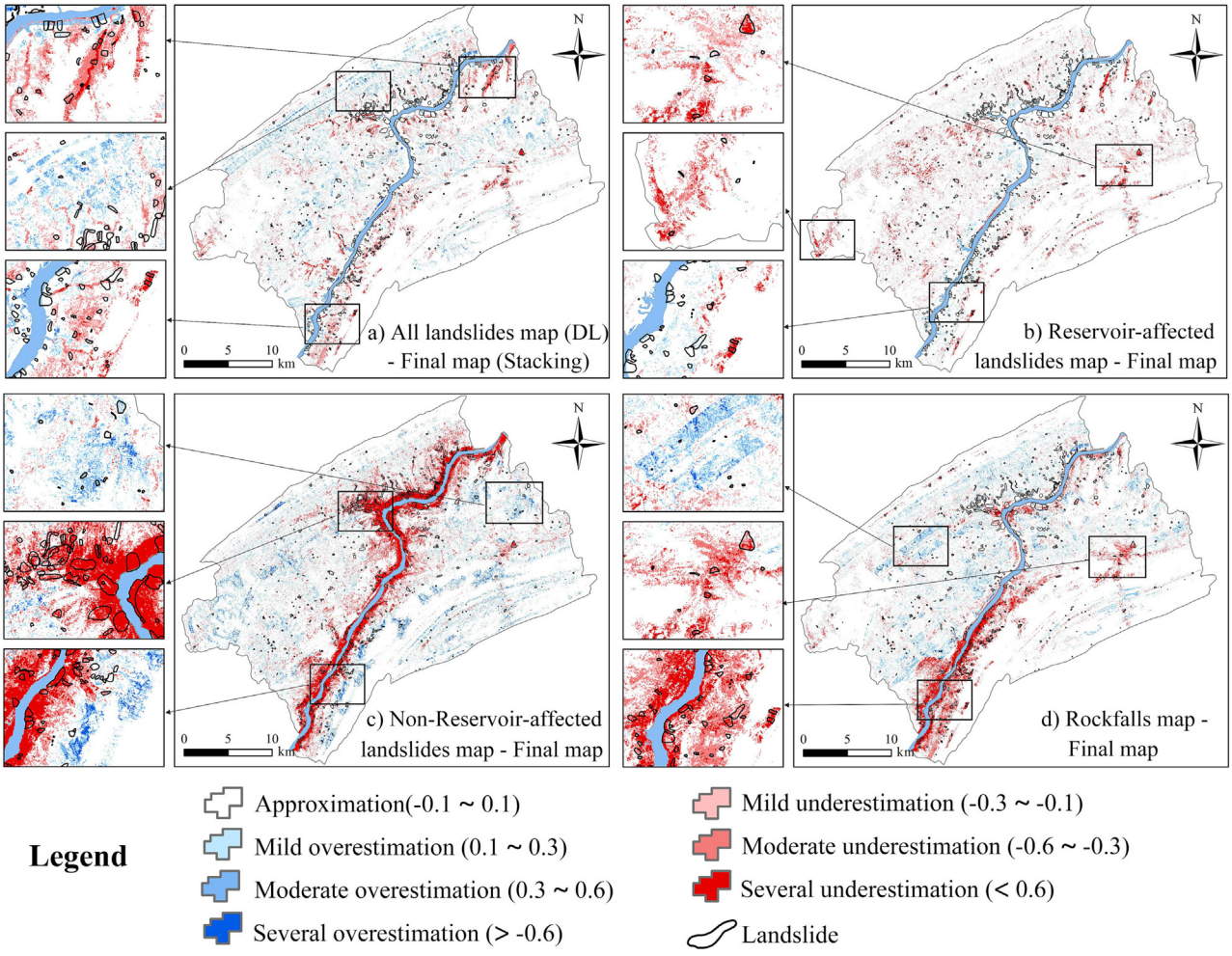

Fig. 15. Comparison map of (a) all landslides map, (b) reservoir-affected landslides map, (c) non-reservoir-affected landslides map, and (d) rockfalls map with the final map, respectively.

Table 7
Statistics of the comparison maps.

Comparison map	Several overestimated	Moderate overestimated	Mild overestimated	Approximation	Several underestimated	Moderate underestimated	Mild underestimated
Fig. 15a	0.18 (**0.02**)	1.57 (0.39)	5.73 (1.45)	82.02 (71.81)	0.60 (**3.83**)	3.36 (9.93)	6.55 (12.56)
Fig. 15b	0.01 (**0.01**)	0.21 (0.32)	1.75 (1.38)	87.61 (81.53)	0.78 (**4.06**)	3.26 (5.15)	6.39 (7.54)
Fig. 15c	0.68 (0.42)	3.16 (1.51)	7.41 (2.55)	70.13 (28.00)	6.09 (45.71)	6.09 (13.39)	6.44 (8.42)
Fig. 15d	0.19 (0.03)	2.03 (0.65)	6.29 (1.66)	78.00 (56.01)	2.45 (15.02)	4.93 (14.56)	6.11 (12.08)

Note: 0.18 (0.02) means Proportion of each comparison level in total area (Proportion of landslide in total landslide).

are located in the southern part of the study area, while the underestimation points are relatively scattered throughout the study area (Fig. 15d).

Based on these four comparison maps and the five landslide susceptibility maps in Section 4.3, we further demonstrate the necessity, reliability and accuracy of considering landslide types when conducting LSM in this study area. In the map modelling without landslide types for all landslides, the LSI of 7.48% pixels is lower than the LSI of the final map (overestimation), and 10.51% pixels is larger than the LSI of the final map (underestimation). This result shows that the susceptibility of study area is slightly decreases after considering landslide types, which is consistent with the conclusion of field survey. A large number of landslides located in the riverside area, leading to the overestimation of susceptibility in that region. Furthermore, we counted the proportion of landslide samples in ten difference levels, and the result shows that after considering landslide types, the LSI of 1.84% landslides samples was decreased, while the LSI of 26.32% landslides samples was increased (Table 7). It can be said that LSM considering different landslide types can effectively improve the accuracy of susceptibility map, especially in areas outside the influence of reservoir water.

As stated in the research of Reichenbach et al. (2018) modelling with limited information on types of landslides has adverse consequences on the practical application of an accurate susceptibility map. We believe that in the TGRA or other similar area with landslides induced by reservoir impoundment, it is significantly necessary to separate reservoir-affected landslides form other landslides in LSM. Several studies have also supported this idea. For example, research by Shu et al. (2021) showed that the accuracy of landslide susceptibility map increased by 1.5% to 5.4% by integrating the landslide susceptibility index of two landslide typologies: shallow landslides and debris flows. Similarly, Zhou et al. (2018) conducted LSM by combining the susceptibility of colluvial landslides and rockfalls in Longju (China), and demonstrated that the separation of landslide types for LSM can improve the prediction accuracy by 0.041 to 0.119. Hence, we suggest that landslides induced by reservoir should be separately recorded to form an event inventory of landslides (proposed by Guzzetti et al. (2006)), which is associated with a triggering event, such as reservoir construction and operation, torrential rainfall, earthquake, or snowmelt event (Liu et al., 2023; Zou et al., 2022).

6. Conclusions

This study presents a new framework for LSM in a mountain-area located in the middle and upper reaches of TGRA, China by considering different landslide types. Firstly, we divided 733 landslides into three types, which are reservoir-affected landslides, non-reservoir-affected landslides, and rockfalls. Next, four landslide inventory datasets and 15 landslide conditional factors were trained by three ML models (LR, RF, SVM), and a DL model (Resnet-18), respectively. Then, the models with highest AUC were used to compute the susceptibility of three types of landslides, respectively, and the Stacking method was designed to integrate the susceptibility of the three types. We compared the susceptibility map considering landslide types with maps of the three types landslides and the map without separating landslide types. All results showed that LSM considering different landslide types effectively improved the accuracy of susceptibility map, with an increase in AUC by 0.041 to 0.119. Overall, this study provides a new approach to achieving high-quality susceptibility mapping in TGRA. High-quality susceptibility maps can help in the implementation of land use planning and reduce the losses caused by landslides. Hence, this study successfully considers the multiple landslide problem in LSM, and provides a new approach for achieving high-quality susceptibility mapping. At the same time, the proposed methodology can effectively map landslide susceptibility in other areas where multiple multi-types of landslides exist. Future research should focus on exploring more unique features associated with different types of landslides and, with the development of ensemble techniques and ML algorithms, make more attempts to build advanced models that consider landslide types for LSM in various environments.

CRediT authorship contribution statement

Lanbing Yu: Conceptualization, Data curation, Methodology, Writing – original draft. **Yang Wang:** Supervision. **Biswajeet Pradhan:** Conceptualization, Supervision, Writing – review & editing.

Declaration of competing interest

The authors declare that they have no known competing financial interests or personal relationships that could have appeared to influence the work reported in this paper.

Acknowledgements

Thanks for the help from Prof. Kunlong Yin in Faculty of Engineering, China University of Geosciences, Wuhan 430074, China, and Qingli Liu from the Geological Environment Monitoring Station of Wanzhou District, Chongqing, China for their assistance.

Appendix A. Supplementary data

Supplementary data to this article can be found online at https://doi.org/10.1016/j.gsf.2024.101802.

References

Al-Najjar, H.A.H., Pradhan, B., 2021. Spatial landslide susceptibility assessment using machine learning techniques assisted by additional data created with generative adversarial networks. Geosci. Front. 12 (2), 625–637. https://doi.org/10.1016/j.gsf.2020.09.002.

Aslam, B., Zafar, A., Khalil, U., 2023. Comparative analysis of multiple conventional neural networks for landslide susceptibility mapping. Nat. Hazards 115 (1), 673–707. https://doi.org/10.1007/s11069-022-05570-x.

Bera, S., Upadhyay, V.K., Guru, B., Oommen, T., 2021. Landslide inventory and susceptibility models considering the landslide typology using deep learning: Himalayas, India. Nat. Hazards 108 (1), 1257–1289. https://doi.org/10.1007/s11069-021-04731-8.

Budimir, M.E.A., Atkinson, P.M., Lewis, H.G., 2015. A systematic review of landslide probability mapping using logistic regression. Landslides 12 (3), 419–436. https://doi.org/10.1007/s10346-014-0550-5.

Camera, C.A.S., Bajni, G., Corno, I., Raffa, M., Stevenazzi, S., Apuani, T., 2021. Introducing intense rainfall and snowmelt variables to implement a process-related non-stationary shallow landslide susceptibility analysis. Sci. Total Environ. 786, 147360-147360. doi: 10.1016/j.scitotenv.2021.147360.

Choi, J., Oh, H.-J., Lee, H.-J., Lee, C., Lee, S., 2012. Combining landslide susceptibility maps obtained from frequency ratio, logistic regression, and artificial neural network models using ASTER images and GIS. Eng. Geol. 124, 12–23. https://doi.org/10.1016/j.enggeo.2011.09.011.

Dai, F.C., Lee, C.F., Ngai, Y.Y., 2002. Landslide risk assessment and management: an overview. Eng. Geol. 64 (1), 65–87. https://doi.org/10.1016/S0013-7952(01)00093-X.

Dou, J., Yunus, A.P., Tien Bui, D., Merghadi, A., Sahana, M., Zhu, Z., Chen, C.-W., Khosravi, K., Yang, Y., Pham, B.T., 2019. Assessment of advanced random forest and decision tree algorithms for modeling rainfall-induced landslide susceptibility in the Izu-Oshima Volcanic Island, Japan. Sci. Total Environ. 662, 332–346. https://doi.org/10.1016/j.scitotenv.2019.01.221.

Dou, J., Yunus, A.P., Bui, D.T., Merghadi, A., Sahana, M., Zhu, Z., Chen, C.-W., Han, Z., Pham, B.T., 2020. Improved landslide assessment using support vector machine with bagging, boosting, and stacking ensemble machine learning framework in a mountainous watershed, Japan. Landslides 17 (3), 641–658. https://doi.org/10.1007/s10346-019-01286-5.

Du, J., Glade, T., Woldai, T., Chai, B., Zeng, B., 2020. Landslide susceptibility assessment based on an incomplete landslide inventory in the Jilong Valley, Tibet, Chinese Himalayas. Eng. Geol. 270, 105572. https://doi.org/10.1016/j.enggeo.2020.105572.

Epifânio, B., Zêzere, J.L., Neves, M., 2014. Susceptibility assessment to different types of landslides in the coastal cliffs of Lourinhã (Central Portugal). J. Sea Res. 93, 150–159. https://doi.org/10.1016/j.seares.2014.04.006.

Erener, A., Mutlu, A., Sebnem Düzgün, H., 2016. A comparative study for landslide susceptibility mapping using GIS-based multi-criteria decision analysis (MCDA), logistic regression (LR) and association rule mining (ARM). Eng. Geol. 203, 45–55. https://doi.org/10.1016/j.enggeo.2015.09.007.

Gorsevski, P.V., Brown, M.K., Panter, K., Onasch, C.M., Simic, A., Snyder, J., 2016. Landslide detection and susceptibility mapping using LiDAR and an artificial neural network approach: a case study in the Cuyahoga Valley National Park, Ohio. Landslides 13 (3), 467–484. https://doi.org/10.1007/s10346-015-0587-0.

Guo, Z., Yin, K., Fu, S., Huang, F., Gui, L., Xia, H., 2019. Evaluation of landslide susceptibility based on GIS and WOE-BP model. Earth Sci. 44 (12), 4299–4312. https://doi.org/10.3799/dqkx.2018.555.

Guzzetti, F., Mihalić Arbanas, S., Reichenbach, P., Sassa, K., Bobrowsky, P.T., Takara, K., 2020. Understanding and Reducing Landslide Disaster Risk: Volume 2 from Mapping to Hazard and Risk Zonation. ICL Contribution to Landslide Disaster Risk Reduction. Springer International Publishing AG, Cham.

Guzzetti, F., Reichenbach, P., Cardinali, M., Galli, M., Ardizzone, F., 2005. Probabilistic landslide hazard assessment at the basin scale. Geomorphology 72 (1), 272–299. https://doi.org/10.1016/j.geomorph.2005.06.002.

Guzzetti, F., Galli, M., Reichenbach, P., Ardizzone, F., Cardinali, M., 2006. Landslide hazard assessment in the Collazzone area, Umbria, Central Italy. Nat. Hazards Earth Syst. Sci. 6 (1), 115–131. https://doi.org/10.5194/nhess-6-115-2006.

Guzzetti, F., Mondini, A.C., Cardinali, M., Fiorucci, F., Santangelo, M., Chang, K.-T., 2012. Landslide inventory maps: New tools for an old problem. Earth-Sci. Rev. 112 (1–2), 42–66. https://doi.org/10.1016/j.earscirev.2012.02.001.

He, K., Zhang, X., Ren, S., Sun, J., 2016. Deep residual learning for image recognition. In: Proceedings of the IEEE Conference on Computer Vision and Pattern Recognition (CVPR), pp. 770–778.

Hong, H., Pourghasemi, H.R., Pourtaghi, Z.S., 2016. Landslide susceptibility assessment in Lianhua County (China): A comparison between a random forest data mining technique and bivariate and multivariate statistical models. Geomorphology 259, 105–118. https://doi.org/10.1016/j.geomorph.2016.02.012.

Hu, Z., Zhu, G., Liu, G., Zhang, B., 2009. The folding time of the eastern Sichuan Jura-type Fold Belt: Evidence from unconformity. Geol. Rev. 55 (1), 32–42. https://doi.org/10.3321/j.issn:0371-5736.2009.01.004.

Huang, F., Chen, J., Liu, W., Huang, J., Hong, H., Chen, W., 2022. Regional rainfall-induced landslide hazard warning based on landslide susceptibility mapping and a critical rainfall threshold. Geomorphology 408, 108236. https://doi.org/10.1016/j.geomorph.2022.108236.

Hungr, O., Leroueil, S., Picarelli, L., 2014. The Varnes classification of landslide types, an update. Landslides 11 (2), 167–194. https://doi.org/10.1007/s10346-013-0436-y.

Lee, S., Min, K., 2001. Statistical analysis of landslide susceptibility at Yongin, Korea. Environ. Geol. 40 (9), 1095–1113. https://doi.org/10.1007/s002540100310.

Liao, M., Wen, H., Yang, L., 2022. Identifying the essential conditioning factors of landslide susceptibility models under different grid resolutions using hybrid machine learning: A case of Wushan and Wuxi counties, China. Catena 217, 106428. https://doi.org/10.1016/j.catena.2022.106428.

Lin, D., Foster, D.P., Ungar, L.H., 2011. VIF regression: A fast regression algorithm for large data. J. Am. Stat. Assoc. 106 (493), 232–247. https://doi.org/10.1198/jasa.2011.tm10113.

Liu, T., Chen, T., Niu, R., Plaza, A., 2021. Landslide detection mapping employing CNN, ResNet, and DenseNet in the Three Gorges Reservoir, China. IEEE J-STARS 14, 11417–11428. https://doi.org/10.1109/JSTARS.2021.3117975.

Liu, S., Wang, L., Zhang, W., He, Y., Pijush, S., 2023. A comprehensive review of machine learning-based methods in landslide susceptibility mapping. Geol. J. 58 (6), 2283–2301. https://doi.org/10.1002/gj.4666.

Loche, M., Alvioli, M., Marchesini, I., Bakka, H., Lombardo, L., 2022. Landslide susceptibility maps of Italy: Lesson learnt from dealing with multiple landslide types and the uneven spatial distribution of the national inventory. Earth-Sci. Rev. 232, 104125. https://doi.org/10.1016/j.earscirev.2022.104125.

Lombardo, L., Cama, M., Conoscenti, C., Märker, M., Rotigliano, E., 2015. Binary logistic regression versus stochastic gradient boosted decision trees in assessing landslide susceptibility for multiple-occurring landslide events: application to the 2009 storm event in Messina (Sicily, southern Italy). Nat. Hazards 79 (3), 1621–1648. https://doi.org/10.1007/s11069-015-1915-3.

Marchesini, I., Ardizzone, F., Alvioli, M., Rossi, M., Guzzetti, F., 2014. Non-susceptible landslide areas in Italy and in the Mediterranean region. Nat. Hazards Earth Syst. Sci. 14 (8), 2215–2231. https://doi.org/10.5194/nhess-14-2215-2014.

Marjanović, M., Kovačević, M., Bajat, B., Voženílek, V., 2011. Landslide susceptibility assessment using SVM machine learning algorithm. Eng. Geol. 123 (3), 225–234. https://doi.org/10.1016/j.enggeo.2011.09.006.

Medina, V., Hürlimann, M., Guo, Z., Lloret, A., Vaunat, J., 2021. Fast physically-based model for rainfall-induced landslide susceptibility assessment at regional scale. Catena 201, 105213. https://doi.org/10.1016/j.catena.2021.105213.

Merghadi, A., Yunus, A.P., Dou, J., Whiteley, J., ThaiPham, B., Bui, D.T., Avtar, R., Abderrahmane, B., 2020. Machine learning methods for landslide susceptibility studies: A comparative overview of algorithm performance. Earth-Sci. Rev. 207, 103225. https://doi.org/10.1016/j.earscirev.2020.103225.

Oh, H.-J., Pradhan, B., 2011. Application of a neuro-fuzzy model to landslide-susceptibility mapping for shallow landslides in a tropical hilly area. Comput. Geosci. 37 (9), 1264–1276. https://doi.org/10.1016/j.cageo.2010.10.012.

Qiu, Y., Zhou, J., 2023a. Short-term rockburst prediction in underground project: insights from an explainable and interpretable ensemble learning model. Acta Geotech. 1–31. https://doi.org/10.1007/s11440-023-01988-0.

Qiu, Y., Zhou, J., 2023b. Short-term rockburst damage assessment in Burst-Prone mines: An explainable XGBOOST hybrid model with SCSO algorithm. Rock Mech. Rock Eng. 56, 8745–8770. https://doi.org/10.1007/s00603-023-03522-w.

Reichenbach, P., Rossi, M., Malamud, B.D., Mihir, M., Guzzetti, F., 2018. A review of statistically-based landslide susceptibility models. Earth-Sci. Rev. 180, 60–91. https://doi.org/10.1016/j.earscirev.2018.03.001.

Samia, J., Temme, A., Bregt, A., Wallinga, J., Guzzetti, F., Ardizzone, F., Rossi, M., 2017. Characterization and quantification of path dependency in landslide susceptibility. Geomorphology 292, 16–24. https://doi.org/10.1016/j.geomorph.2017.04.039.

Segoni, S., Pappafico, G., Luti, T., Catani, F., 2020. Landslide susceptibility assessment in complex geological settings: sensitivity to geological information and insights on its parameterization. Landslides 17 (10), 2443–2453. https://doi.org/10.1007/s10346-019-01340-2.

Sharma, L.P., Patel, N., Ghose, M.K., Debnath, P., 2015. Development and application of Shannon's entropy integrated information value model for landslide susceptibility assessment and zonation in Sikkim Himalayas in India. Nat. Hazards 75 (2), 1555–1576. https://doi.org/10.1007/s11069-014-1378-y.

Shou, K.-J., Chen, J., 2021. On the rainfall induced deep-seated and shallow landslide hazard in Taiwan. Eng. Geol. 288, 106156. https://doi.org/10.1016/j.enggeo.2021.106156.

Shu, H., Guo, Z., Qi, S., Song, D., Pourghasemi, H., Ma, J., 2021. Integrating landslide typology with weighted frequency ratio model for landslide susceptibility mapping: A case study from Lanzhou city of northwestern China. Remote Sens. 13 (18), 3623. https://doi.org/10.3390/rs13183623.

Silva, R., Marques, R., Gaspar, J., 2018. Implications of landslide typology and predisposing factor combinations for probabilistic landslide susceptibility models: A case study in Lajedo Parish (Flores Island, Azores—Portugal). Geosciences 8 (5), 153. https://doi.org/10.3390/geosciences8050153.

Smyth, P., Wolpert, D., 1999. Linearly combining density estimators via stacking. Mach. Learn. 36 (1), 59–83. https://doi.org/10.1023/A:1007511322260.

Tang, H., Wasowski, J., Juang, C.H., 2019. Geohazards in the three Gorges Reservoir Area, China – Lessons learned from decades of research. Eng. Geol. 261, 105267. https://doi.org/10.1016/j.enggeo.2019.105267.

Tekin, S., Çan, T., 2022. Slide type landslide susceptibility assessment of the Büyük Menderes watershed using artificial neural network method. Environ. Sci. Pollut. Res. 29 (31), 47174–47188. https://doi.org/10.1007/s11356-022-19248-1.

Temme, A., Guzzetti, F., Samia, J., Mirus, B.B., 2020. The future of landslides' past—a framework for assessing consecutive landsliding systems. Landslides 17 (7), 1519–1528. https://doi.org/10.1007/s10346-020-01405-7.

Thiery, Y., Malet, J.P., Sterlacchini, S., Puissant, A., Maquaire, O., 2007. Landslide susceptibility assessment by bivariate methods at large scales: Application to a complex mountainous environment. Geomorphology 92 (1), 38–59. https://doi.org/10.1016/j.geomorph.2007.02.020.

Tien Bui, D., Tuan, T.A., Klempe, H., Pradhan, B., Revhaug, I., 2016. Spatial prediction models for shallow landslide hazards: a comparative assessment of the efficacy of support vector machines, artificial neural networks, kernel logistic regression, and logistic model tree. Landslides 13 (2), 361–378. https://doi.org/10.1007/s10346-015-0557-6.

Tofani, V., Bicocchi, G., Rossi, G., Segoni, S., D'Ambrosio, M., Casagli, N., Catani, F., 2017. Soil characterization for shallow landslides modeling: a case study in the Northern Apennines (Central Italy). Landslides 14 (2), 755–770. https://doi.org/10.1007/s10346-017-0809-8.

Valdés Carrera, A.C., Mendoza, M.E., Carlón Allende, T., Macías, J.L., 2022. Multitemporal landslide inventory analysis of an intertropical mountain in west-central Mexico — Basis for hazard management. J. MT Sci.-Engl. 19 (6), 1650–1669. https://doi.org/10.1007/s11629-021-7223-3.

van den Bout, B., Tang, C., van Westen, C., Jetten, V.G., 2022. Physically based modeling of co-seismic landslide, debris flow, and flood cascade. Nat. Hazards Earth Syst. Sci. 22 (10), 3183–3209. https://doi.org/10.5194/nhess-22-3183-2022.

Wang, L., Wu, C., Yang, Z., Wang, L., 2023. Deep learning methods for time-dependent reliability analysis of reservoir slopes in spatially variable soils. Comput. Geotech. 159, 105413. https://doi.org/10.1016/j.compgeo.2023.105413.

Xiao, T., Yin, K., Yao, T., Liu, S., 2019. Spatial prediction of landslide susceptibility using GIS-based statistical and machine learning models in Wanzhou County, Three Gorges Reservoir, China. Acta Geochimica 38 (5), 654–669. https://doi.org/10.1007/s11631-019-00341-1.

Xiao, T., Segoni, S., Chen, L., Yin, K., Casagli, N., 2020. A step beyond landslide susceptibility maps: a simple method to investigate and explain the different outcomes obtained by different approaches. Landslides 17 (3), 627–640. https://doi.org/10.1007/s10346-019-01299-0.

Xu, H., Liu, Y.-Q., Kuang, H.-W., Liu, Y.-X., Peng, N., 2017. Jurassic-Cretaceous terrestrial transition red beds in northern North China and their implication on regional paleogeography, paleoecology, and tectonic evolution. Palaeoworld 26 (2), 403–422. https://doi.org/10.1016/j.palwor.2016.05.007.

Yin, K., 1990. Statistical prediction models for slope instability of metamorphosed rocks. Int. J. Rock Mech. Min. Sin. Geomech. Abstr. 27 (1), 43. https://doi.org/10.1016/0148-9062(90)90358-9.

Youssef, A.M., Pradhan, B., Dikshit, A., Al-Katheri, M.M., Matar, S.S., Mahdi, A.M., 2022. Landslide susceptibility mapping using CNN-1D and 2D deep learning algorithms: comparison of their performance at Asir Region, KSA. Bull. Eng. Geol. Environ. 81 (4). https://doi.org/10.1007/s10064-022-02657-4.

Yu, L., Zhou, C., Wang, Y., Cao, Y., Peres, D.J., 2022. Coupling data- and knowledge-driven methods for landslide susceptibility mapping in human-modified environments: A case study from Wanzhou County, Three Gorges Reservoir Area, China. Remote Sens. 774. https://doi.org/10.3390/rs14030774.

Yuan, R., Chen, J., 2022. A hybrid deep learning method for landslide susceptibility analysis with the application of InSAR data. Nat. Hazards 114 (2), 1393–1426. https://doi.org/10.1007/s11069-022-05430-8.

Zêzere, J.L., 2002. Landslide susceptibility assessment considering landslide typology. A case study in the area north of Lisbon (Portugal). Nat. Hazards Earth Syst. Sci. 2 (1/2), 73–82. https://doi.org/10.5194/nhess-2-73-2002.

Zhang, J., Yin, K., Wang, J., Liu, L., Huang, F., 2016. Evaluation of landslide susceptibility for Wanzhou district of Three Gorges Reservoir. Chinese Journal of Rock Mechanics and Engineering 35, 284–296. https://doi.org/10.13722/j.cnki.jrme.2015.0318 (in Chinese with English abstract).

Zhang, W., Li, H., Han, L., Chen, L., Wang, L., 2022a. Slope stability prediction using ensemble learning techniques: A case study in Yunyang County, Chongqing, China. J. Rock Mech. Geotech. Eng. 14 (4), 1089–1099. https://doi.org/10.1016/j.jrmge.2021.12.011.

Zhang, W., Li, H., Tang, L., Gu, X., Wang, L., 2022b. Displacement prediction of Jiuxianping landslide using gated recurrent unit (GRU) networks. Acta Geotech. 17, 1367–1382. https://doi.org/10.1007/s11440-022-01495-8.

Zhang, W., Wu, C., Tang, L., Gu, X., 2023. Efficien Optimization of random forest through the use of MVO, GWO and MFO in evaluating the stability of underground entry-type excavations t time-variant reliability analysis of Bazimen landslide in the Three Gorges Reservoir Area using XGBoost and LightGBM algorithms. Gongwana Res. 123, 41–53. https://doi.org/10.1016/j.gr.2022.10.004.

Zhou, C., Yin, K., Cao, Y., Ahmed, B., Li, Y., Catani, F., Pourghasemi, H.R., 2018. Landslide susceptibility modeling applying machine learning methods: A case study from Longju in the Three Gorges Reservoir area, China. Comput. Geosci. 112, 23–37. https://doi.org/10.1016/j.cageo.2017.11.019.

Zhou, C., Cao, Y., Yin, K., Intrieri, E., Catani, F., Wu, L., 2022a. Characteristic comparison of seepage-driven and buoyancy-driven landslides in Three Gorges Reservoir area, China. Eng. Geol. 301, 106590. https://doi.org/10.1016/j.enggeo.2022.106590.

Zhou, J., Huang, S., Qiu, Y., 2022b. Optimization of random forest through the use of MVO, GWO and MFO in evaluating the stability of underground entry-type excavations. Tunn. Undergr. Sp. Tech. 124, 104494. https://doi.org/10.1016/j.tust.2022.104494.

Zhou, X., Wen, H., Zhang, Y., Xu, J., Zhang, W., 2021. Landslide susceptibility mapping using hybrid random forest with GeoDetector and RFE for factor optimization. Geosci. Front. 12 (5), 101211. https://doi.org/10.1016/j.gsf.2021.101211.

Zhu, A.X., Wang, R., Qiao, J., Qin, C.-Z., Chen, Y., Liu, J., Du, F., Lin, Y., Zhu, T., 2014. An expert knowledge-based approach to landslide susceptibility mapping using GIS and fuzzy logic. Geomorphology 214, 128–138. https://doi.org/10.1016/j.geomorph.2014.02.003.

Zou, Y., Qi, S., Guo, S., Zheng, B., Zhan, Z., He, N., Huang, X., Hou, X., Liu, H., 2022. Factors controlling the spatial distribution of coseismic landslides triggered by the Mw 6.1 Ludian earthquake in China. Eng. Geol. 296, 106477. https://doi.org/10.1016/j.enggeo.2021.106477.